APPLICATION OF MULTIPULSE EXCITATION TO STUDY EXOCYTOTIC PROCESSES IN CELLS STAINED WITH ACRIDINE ORANGE

by

DMYTRO SHUMILOV

Bachelor of Science, 2010
Kharkiv National University
Kharkiv, Ukraine

Master of Science, 2013
Texas Christian University
Fort Worth, TX

Submitted to the Graduate Faculty of the
College of Science and Engineering
Texas Christian University
In partial fulfillment of the requirements
for the degree of

Doctor of Philosophy

May 2014

ACKNOWLEDGMENTS

To my advisor, Dr. Gryczynski, gratitude is expressed for his support and participation.

Thanks to Dr. Zerda for his corrections to the thesis. Thanks to Dr.Grygorczyk for his management of the cell imaging experiments.

TABLE OF CONTENTS

LIST OF FIGURES

LIST OF TABLES

INTRODUCTION

Over the last decades fluorescence has become one of the major technologies for studying biological systems [1,2]. Its main advantages are: the outstanding sensitivity (it can measure a single molecule of a biological substance), very high temporal resolution (down to a few picoseconds), high spatial resolution (recently reaching below 100 nm), fast and easy detection of biological molecules, and a relatively low cost as compared to other technologies, for example, nuclear magnetic resonance (NMR) or mass spectrometry (MS) [3,4]. There are two important features that make fluorescence applications very advantageous [5]. Fluorescent molecules absorb light of a certain energy (wavelength) and emit light of a different (lower) energy (and longer wavelength). This difference between the absorbed and the emitted energy/wavelength is called Stoke's shift, and it allows a simple rejection of the excitation light background, dramatically increasing the detection sensitivity. Also, the emission event is independent from the absorption event, and is separated in time. This time separation when a molecule is in an excited state is called fluorescence lifetime [6,7]. The fluorescence lifetimes for different molecules may range from a few picoseconds to tens of nanoseconds. During this time molecules interact with the environment surrounding them and reorient themselves, and the emitted fluorescence photons bring in the information about these processes [8,9,10]. The ability of fluorescence to bring in the information about the surroundings and dynamics of the system makes the measurements of fluorescence energy and fluorescence lifetimes a very powerful technology with many applications in chemistry, biology, and medical diagnostics [11, 12]. Another important benefit of fluorescence lifetime measurements is the fact that this technique fits to a microscopy allowing the observation of cellular and subcellular processes [13, 14,15]. Since a typical low intensity visible infrared and near-infrared (NIR) light is harmless for biological systems it is possible to monitor biological processes *in-vivo* for a long time [16,17,18, 19].

Very few naturally occurring molecules are fluorescent [20]. The most known natural fluorescent molecules are Tryptophan and Tyrosine. They belong to a group of natural amino acids that absorb and emit in the UV spectral range. Due to this property, Tryptophan and Tyrosine amino acids are widely used but only for *in-vitro* and *in-vivo* protein studies [21, 22]. In the last 30 years a new group of naturally fluorescent proteins has emerged. Green Fluorescent Protein (GFP), a highly fluorescent visible range (green) protein, was first isolated from *Aequorea victoria* [23]. In the last 15 years the field of fluorescent proteins has virtually exploded with numerous new fluorescent proteins ranging from blue to red. This brought in many biological applications that have been driving new biophysical and medical discoveries. The incredible range of biological applications of GFP and fluorescence techniques was recognized in 2008 with the award of a Noble Prize in chemistry.

Since the number of naturally occurring fluorescent molecules is rather limited, the development of various artificial fluorescent substances called dyes is a main focus of probe chemistry. Availability of the fluorescent dyes/probes is still a limiting step for many practical uses and applications of fluorescence. Biomedical diagnostics and fluorescence-based sensing has recently become the main incentive for probe development [20]. The possibility of detecting extremely low concentrations of analytes (samples of interest) in the amount of femtomoles and smaller, in a very small volume (femtoliters) opens the road for many new biophysical applications. One of the most prominent applications of the fluorescence techniques is genomics (DNA sequencing) where fluorescence detection plays a fundamental role. Genomic projects and broad biomedical applications of fluorescence have been stimulating probe development for over 25 years [21,22].

In the last 15 years we have also been witnessing the emergence of fluorescence applications to living cells. Increasing availability of fluorescent probes and fluorescent proteins opens new ways for studying molecular processes on a cellular level [21, 22].

To investigate specific molecular/cellular processes we have to select/develop adequate dyes and a fluorescence technology that most accurately detects the process we want to observe. For example, to study pH distribution inside a cell one would search for dyes that are water soluble and whose fluorescence signals are sensitive to the pH concentrations within the physiological pH range. In order to study membrane processes one would look for probes that will penetrate into a non-polar lipid environment [24].

One physiological process that has recently become an object of scientific studies is mucus secretion and expansion [25]. Physiologically mucus is the first-line of defence against the barrage of irritants inhaled into the lungs during breathing [26, 27]. Mucus forms a thin film of viscoelastic gel on the surface of the airways that protect the epithelial cells by entrapping foreign bodies, i.e. debris, bacteria, and viruses, and clearing them from the airway by ciliary movement, a process termed mucociliary clearance [28, 29, 30]. In some diseases, such as cystic fibrosis (CF), asthma, and chronic obstructive pulmonary disease (COPD), excessive production of mucus (hypersecretion), as well as changes in its viscoelastic properties results in the accumulation of thick, sticky mucus in the lungs, effectively impairing the mucociliary clearance process. This leads to difficulty in breathing, morbidity, and in severe cases, mortality [31,32]. Mucus gel is comprised of 1% to 2% of mucin glycoproteins that are secreted by specialized cells. Mucus gel consists of polyanionic macromolecules that are stored in cytoplasmic granules in a highly condensed state. Upon stimulation they are rapidly secreted, in tens of a millisecond, by the exocytotic process and undergo enormous, several-hundred-fold swelling/expansion [33].

Mucus is a colorless substance, and any microscope-based approach will suffer from the lack of sufficient color contrast necessary for the visual scrutiny of the substance. Because of this *in-vivo* studies of mucus release are limited, and we still lack a basic understanding of this process. Detecting, studying, and understanding the regulatory mechanisms of mucus swelling will play a fundamental role in the development of the cure for Cystic Fibrosis and prevention of many respiratory diseases [32,33].

We have recently reported an interesting observation [34, 35] of Acridine Orange (AO) dye that accumulates in high concentrations in cellular vesicles. When it is released, the expansion of mucus results in significant dilution of AO. In high concentrations AO forms aggregates that have spectroscopic properties very different from those of the monomeric form. A change in the aggregate-monomer equilibrium reflects the mucus dilution process and can be monitored by fluorescence. At this stage, two AO effects are observed. One is a change of AO in color – aggregates have a longer emission wavelength centered at about 640 nm (red color) as opposed to the emission of monomers that is centered at about 530 nm (green/yellow color). The second is a dramatic change in AO's fluorescence lifetime. Monomers of AO (diluted form) have a fluorescence lifetime of about 1.7 ns while the aggregates have a fluorescence lifetime of about 20 ns. Such a dramatic difference in the fluorescence lifetimes offers an excellent opportunity for the Fluorescence Lifetime Imaging Microscopy (FLIM).

FLIM measurements are considered to be the most sensitive and the most suitable for cellular imaging. Unfortunately, the emission intensity of AO aggregates is relatively weak (about 5-10 fold weaker than those from the monomers) [34], and even the small fraction of monomers, while emitting their signal, quickly overwhelms the aggregates' signal. Thus, detecting a small fraction of AO aggregates in a quickly expanding mucus becomes a significant technical challenge.

In this work we are presenting a new approach to the time-resolved measurements that allow a significant increase in sensitivity to the AO aggregates signal while detecting small fractions of long-lived species (in our case the aggregates mentioned above). By applying a newly developed multi-pulse excitation approach we can increase the contribution of the long-lived fluorescence species to the emission. This way we can significantly increase the detection sensitivity to the long-lived AO aggregates that will allow the monitoring of mucus expansion for a much longer period of time (for the much smaller concentrations of aggregates diluted in mucus).

BACKGROUND

Motivation

Lung mucus has a number of functions in the human airways, including its central role in trapping and clearing bacteria and external agents. Malfunction in the mucus swelling processes causes thick, sticky mucus accumulation on the epithelial tissue of the lungs. This type of mucosal defect is a symptom of chronic obstructive pulmonary disease (COPD) and cystic fibrosis (CF). Mechanisms of mucus release and swelling have recently been a focus of multiple experiments performed to understand the causes of the process malfunction that typically leads to thick and viscos mucus. Malfunctions in the swelling process have recently been implicated in disease conditions, such as cystic fibrosis (CF), asthma, and chronic obstructive pulmonary disease (COPD), where the excessive production of mucus (hypersecretion) and changes in its biophysical properties (viscoelasticity) result in accumulation of thick, sticky mucus in the lungs, effectively impairing the mucociliary clearance process. This in turn leads to infections, difficulty in breathing, morbidity, and in severe cases, mortality [32,33,35].

There are a number of studies that have been done in the last few decades with the goal of revealing the structure and the properties of mucus. Phenomena of mucus formation can be viewed from different angles. Improper functionality of mucus secretion due to swelling of a system can cause severe symptoms that affect normal functionality of lungs as mentioned before. The matrix of gels forms a supramolecular network with properties that cannot be understood solely on the basics of the properties of the molecules that make it. Polymers interact with each other when they lie close in the matrix. One of the oldest and the most important questions is whether mucin is a chemical gel, where branched polymers interact with each other by the covalent S:S bond, or whether it is a physical gel where polymers interact due to low energy electrostatic and hydrophobic bonds and mechanical tangles. Both of these points of view can turn out to be correct.

Mucus is not only present as a defensive mechanism in the lungs, but it resides in the gastrointestinal tract as well. Gastrointestinal mucus is more condensed and has different rheological properties than lung mucus; it is thicker and denser. This fact can be related to different topology of the mucus gel. Rheological properties of chemical gels depend on the degree of the covalent cross-links between polymer chains, so defective s - s bonding can be a source of mucus malfunction. On the other hand, rheological properties of physical gels depend on the degree of swelling (number of tangles per unit volume) of the mucus. Tangles are formed as a result of physical interaction between mucins. In this case, improper swelling would cause the mucus pathology. Since mucus stays in the condensed state in the granules and then is released into the intracellular space, swelling is a necessary stage in mucus layer formation on the epithelial cells [31, 32, 33].

Since there is no chemical bonding between the proteins and the interaction of the mucins depends on tangles. If a mucus gel matrix is tangled, it will quickly relax to the equilibrium, so its swelling will depend on the volume of water available in the system (or on any other solvent). Rheological properties of the tangled-matrix gels depend on the tangles density, and interchain tangles decrease exponentially when the mucus volume grows, small changes in swelling equilibrium result in large changes in mucus rheology and improper swelling becomes a main cause of the pathology.

On the other hand, epithelial tissue of the lung cells also contains cilia that are beating and thus facilitating mucus clearance. The system of the epithelial tissue consists of two components: mucus that traps viruses, bacteria, dust particles and toxicants and a periciliary layer (PCL) that provides the clearance of the mucus out of the lungs. The periciliar layer consists of the beating cilia and a certain environment that provides a possibility for the cilia beating and lubrication of the cell-surface layer. Modern models that describe the process of the cilia beating and mucus clearance assume that the PCL consists of the environment that ensures the cilia beating and provides the cilia themselves that participate in this process. The environment for the proper cilia movement has to be non-viscous to provide proper beating of the cilia and the mucus clearance as the result of this process. On the other hand, mucus lying on the top of the cilia should not penetrate into the periciliar layer as demonstrated in the experiment recently published in [36].

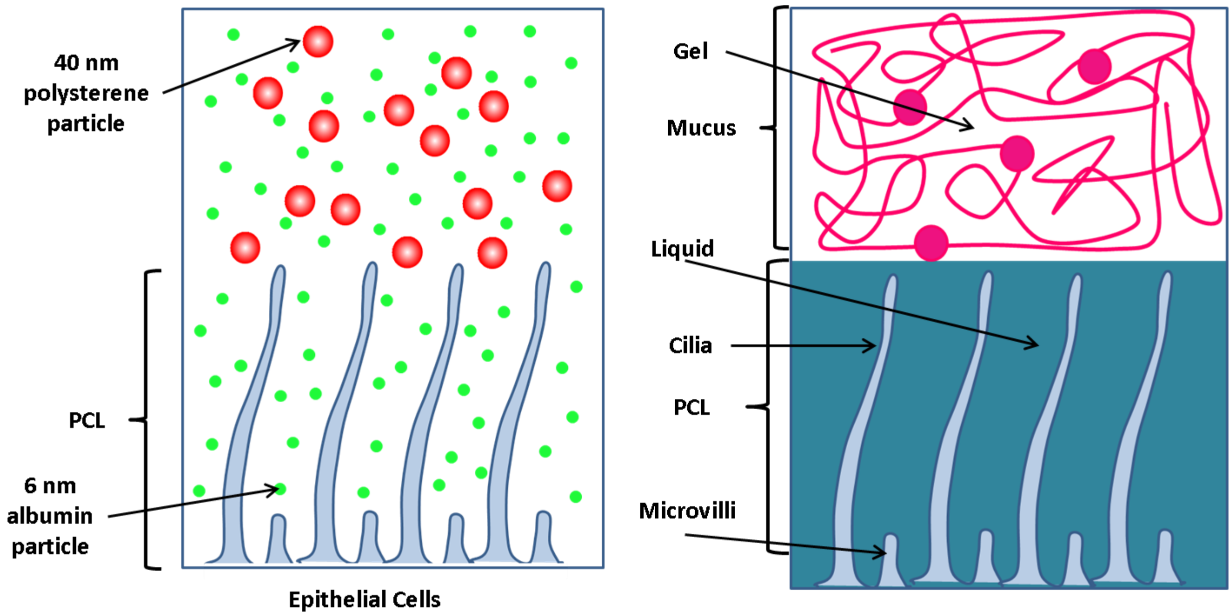

Figure 1. Gel on liquid model for the beating cilia in human lungs with demonstration of the experiment with albumin particles

For a long time a gel-on-liquid model was accepted. It considered a low-viscosity liquid layer, which facilitates the efficient ciliary beating [36,37,38]. Experiments with beating cilia and immobile cilia have demonstrated that a gel-on-liquid model is not quite correct and a gel-on-brush model of the airway surface was introduced. This model better explains the mucus clearance process. In an experiment the cilia were immobilized artificially with the purpose of stopping mucus clearance. Two types of particles with different sizes were used in this experiment. The smaller albumin particles of 6nm size were able to penetrate the PCL layer, but the bigger polysterine particles of 40 nm size were not able to penetrate this layer. As a result it was possible to see that in case of the immobile cilia mucus accumulates on the airway surface and clearance is constrained. The high viscosity of mucus that prevents cilia from beating can cause mucus clearance malfunction. As was discussed before, mucus layer formation is a result of the swelling/expansion of mucus after it has been released from the epithelial cells leading to the formation of a uniform protection layer. The structure of lung mucus proteins has been studied with crystallography and/or transmission electron microscopy (TEM). But these technologies only show static information and cannot reveal dynamics of the release and swelling process. In order to study the kinetics of the exocytotic release process and mucus expansion into a uniform epithelial layer it is necessary to have an appropriate probe and technology that is capable of monitoring the quickly expanding mucin protein. This expansion process is very fast and lasts milliseconds, during which the protein increases its volume few hundred times.

Recently it was observed that AO could gather in high concentration in cellular vesicles that have lower pH [34]. Interestingly, this concentration is sufficient to form AO aggregates that present red long-lived emission. Our fluorescence confocal microscopy studies clearly indicate presence of AO aggregates [36]. We also observed that when vesicles release their contents into the extracellular space, mucus expands significantly and quickly dilutes the accumulated AO. Since the aggregate-monomer equilibrium is a very fast process (occurring within microseconds) the volume increase and the AO dilution will be reflected in the relative fractions of monomers and aggregates. Since the emission wavelength and fluorescence lifetimes of the AO-aggregates are very different from those of the AO-monomers, by measuring fluorescence lifetimes at different observation wavelengths (530 nm monomers and 640 nm aggregates) we can obtain very precise information on the aggregate/monomer ratio (relative contribution) that accurately reflects the AO dilution. By applying time-resolved Total Internal Reflection Fluorescence (TIRF) microscopy we will be able to quantitatively monitor the mucus release process on the cellular level and explore mucus formation pathology.

For the last couple of years we have been studying AO properties in the view of its potential application to the mucus expansion processes. My Master's thesis presents results characterizing Acridine Orange as a fluorescent probe to study cellular processes. These included the basic spectroscopic properties, molar extinction coefficient, quantum yield, and absorption and emission spectra. These recently published results [36] have demonstrated the potential of AO and that it can be used to study the lung mucus exocytotic and expansion processes.

Preliminary results presented by us [34,35,36] have indicated that after the initial granules release the concentration of AO and fraction of aggregates drops very quickly making precise quantitative detection of the aggregates very difficult.

The emission of aggregates is about 640 nm, it is shifted toward the red and its fluorescence lifetime is over 10 times longer than the lifetime of monomers. But the brightness of the AO aggregates is over 20 times lower than the brightness of the monomers (the quantum yield of the aggregates is about 10 times lower than for monomers and the extinction coefficient is more than 2 times lower than for monomers) and detecting small fractions of the AO aggregates can be a significant challenge. We were looking for an approach that would allow exposing a long-lived emission with the background of a short emission. One existing approach to solve this problem is time-gated detection. The idea for time-gated detection was developed over 20 years ago and has being used very successfully in cellular and tissue imaging for background and scattering elimination. The concept is to start the detection a fixed time after the excitation pulse (Figure 2). Scattering and fluorescence intensities for species with short fluorescence lifetimes decay quickly while the intensity of the long-lived species decays much more slowyl. Detection started a short time after the pulsed excitation will detect a higher relative fraction of the long component of the spectrum.

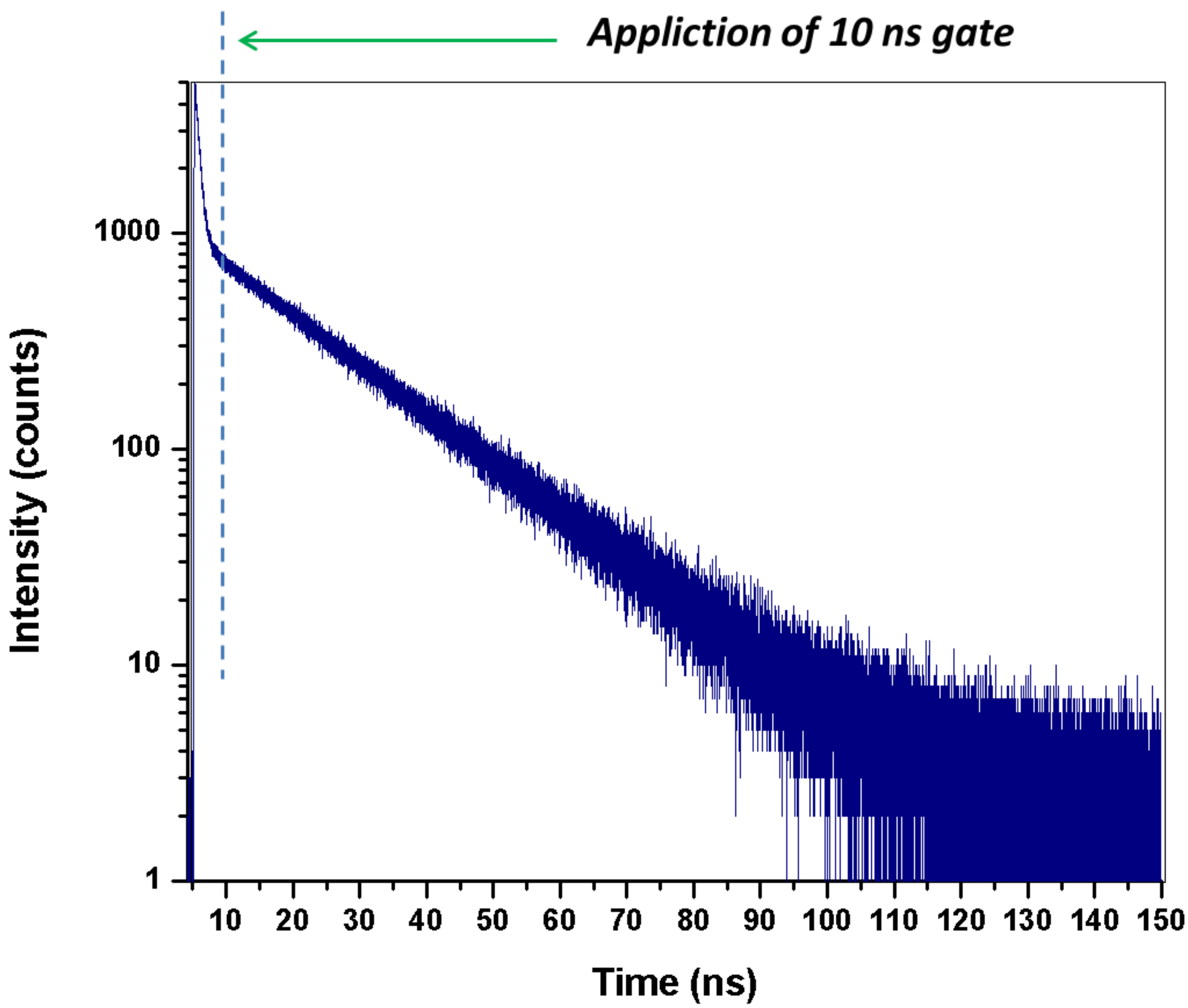

Figure 2. Schematics of gated detection

The drawback of such an approach is that by delaying the signal we are sacrificing a significant portion of the useful emission intensity. In fact, all photons before the gate start time are lost. This is not a problem if one can easily increase the initial signal to compensate for the loss.

We can significantly increase the signal of the long lived component by using a multiple pulse excitation approach. The concept was originally tested with the long lived Ruthenium probe (Rubpy) that has a fluorescence lifetime of 350 ns. We demonstrated [39] that using 40 pulses 80 MHz increase the initial intensity of Ruthenium more than 20 times as compared to a single pulse excitation. While at the same time the signal from the short lived fluorescein background (about 4 ns fluorescence lifetime) does not change at all.

Our initial simulations indicate that we can achieve significant enhancement (pumping) of species with the 20 ns lifetime, but the required repetition needs to be over 300 MHz. The typical repetition of the excitation laser diodes and lasers are 80 MHz and lower. There are no easily obtainable excitation sources that can produce pulses with a frequency over 100 MHz. Currently we are searching for an approach that will allow increasing the repetition rate to a desirable range. Herein we are presenting a simple approach that allows generating a burst of pulses with an internal repetition rate much over 100 MHz. We demonstrate that for our AO system with a lifetime of 20 ns (for aggregates) and 1.8 ns (for monomers) using ~ 300 MHz repetition rate in the burst we can significantly increase the initial signal of long lived aggregates that in turn will allow detection of significantly higher dilutions.

Acridine Orange

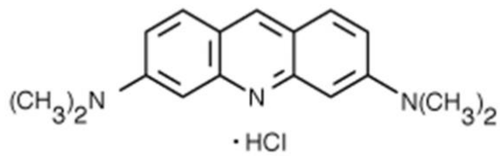

Figure 3. Molecular structure of Acridine Orange

Acridine Orange (AO) is a well-known DNA intercalator [40,41,42] and has been used for DNA studies for over 20 years. Intercalation is the reversible inclusion of a molecule between two other molecules (DNA base in this case). Intercalation can be monitored by fluorescence emission. At low concentrations, (starting at 200nM) AO spectra are similar to those of fluorescein, an organic fluorescence dye. It has an absorption maximum around 494 nm and an emission wavelength of 525 nm. When AO binds to DNA or RNA, the emission properties change significantly and the emission peak will shift to 640 nm.

Acridine Orange (AO) is a fluorescent dye that also accumulates in the cellular vesicles that have lower pH (5.5). At high concentration (105mM) it forms aggregates and at the lower concentrations (200nM and below) mostly monomeric form is present. AO as shown in Figure 3 has molecular weight of 265.35 g/mol.

Figure 4. Accumulation of the high concentration of AO in the Calu3 cell mucosal granule

Fraction of dimers and monomers in the solution changes with the decrease of the concentration. Emission properties of dimers and monomers are different as are their lifetimes. This fact allows us to detect and monitor mucus granule release and the mucus expansion process with the help of Acridine Orange. Mucus mostly consists of mucins, glycoproteins that are densely packed in the granulas. During the excocytotic process packed mucins are released into the extracellular space and unfold, forming a uniform layer on the surface of the epithelial cells. When mucins unfold, they increase their volume by a factor of a few hundred. Acridine Orange, which is released together with mucins will occupy the same volume and decrease its concentration by a factor of a few hundred. Such concentration changes can be monitored by measuring changes in the fluorescent properties of Acridine Orange [34].

Fluorescence Emission

Fluorescent molecules have complex electronic structures. Molecules which are excited as a result of the absorption of photons tend to return to the ground state. Processes that take place between the absorption and emission of a photon are described below on the Perrin – Jablonski diagram:

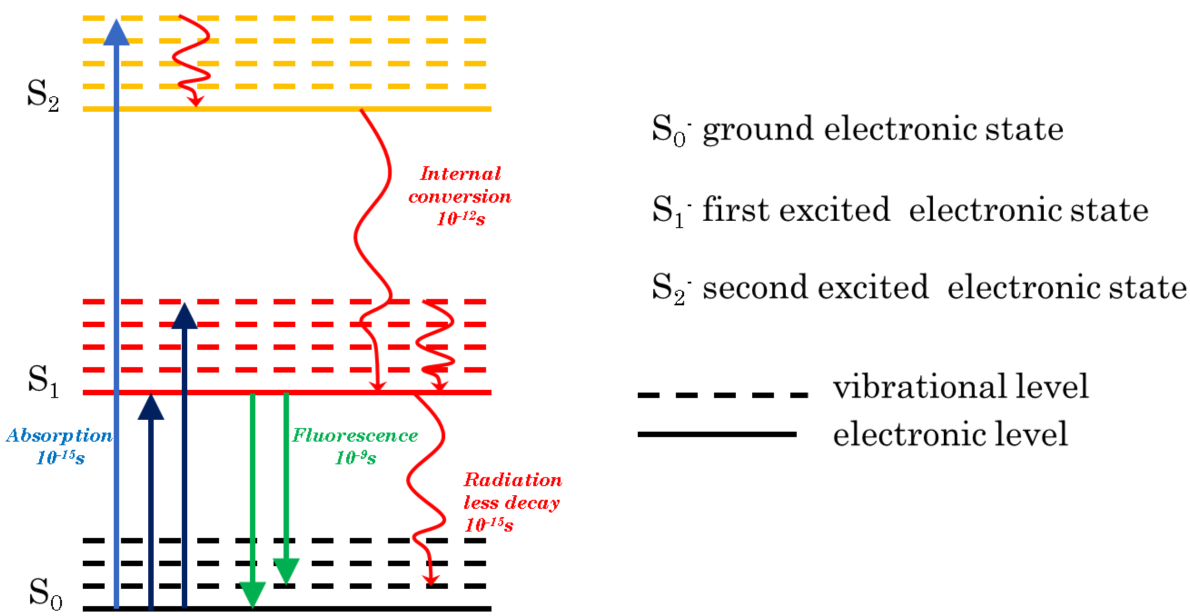

Figure 5. Perrin - Jablonski diagram

The electronic states on the diagram are marked as: *S_0 – ground state, S_1 – first excited state,* and *S_2 – second excited state* respectively. The excited molecule can also exist in a number of vibrational states, which are transient and are shown on the diagram using dashed lines. Vertical straight lines describe processes that promote radiative absorption or emission of a photon. Deactivation of the excited state can be radiative as well as nonradiative, so emission of a photon is not a necessary condition for a molecule to return to the ground state. Internal conversion takes place when a molecule relaxes from some vibrational level of S_1 or S_2 to the lowest excited vibrational level S_1. Rate of this process is approximately $10^{12}s^{-1}$.

Excited fluorescent molecules return to the ground state as a result of the emission process. Emission takes place from the lowest excited level S_1. Molecules return directly to the ground state S_0 or one of its vibrational levels. Kasha's rule states that fluorescence emission spectra do not depend on the excitation wavelength, which follows from the description above. Excited fluorescent molecules emit photons at longer wavelength than the excitation wavelength. This phenomenon occurs because some energy is lost while the molecule is in the excited state and then the energy of the emitted photon is lower than the energy of the absorbed photon. The concept for a Stoke's shift is shown in Figure 6 [43,44]. Stokes shift is the difference between absorption and emission bands' maximum values. It demonstrates energy loss of the emitted photon.

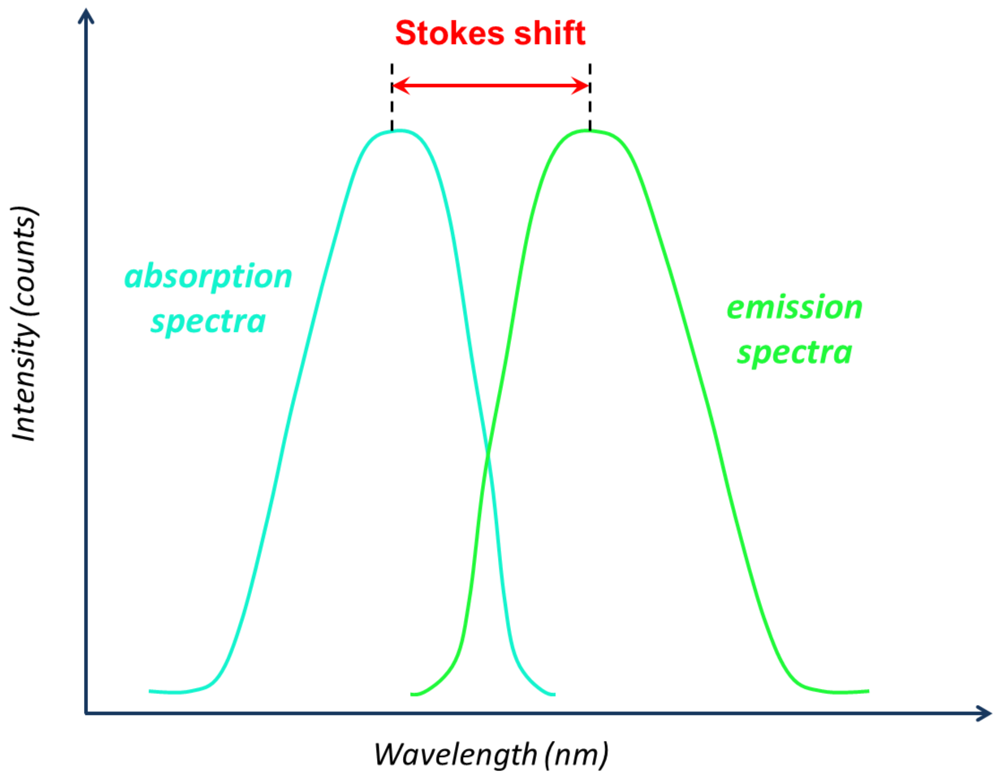

Figure 6. Stoke's shift that can be observed between absorption and emission measurements

Fluorescence Lifetime

An important characteristic of fluorescence is a significant finite time between the excitation process and the emission process called fluorescence lifetime. As mentioned before, the rates for deactivation of the excited singlet state are providing lifetimes that are typically on the order of nanoseconds. Importantly deactivation of the excited state is a statistical process and fluorescence lifetime represents the average time a molecule spends in the excited state. The fluorescence lifetime contains information about the molecule (a fluorophore) and is independent from many factors such as excitation wavelength, excitation power, and to a large extent, molecular concentration. Because of that it might provide important information about the molecular system. For example, multi-exponential decay can supply information about the intermolecular interaction of a fluorophore with a solvent or various complex formations. Macromolecules often can exist in different conformations, and multi- exponential decays of a fluorophore can give information about the number of conformational states. The fluorescence lifetime can be expressed through deactivation rates as:

$$\tau = \frac{1}{\Gamma + k_{nr}} \tag{1}$$

The lifetime τ describes an average time that molecules spend in the excited state. If we assume that initially $N_0=N(t_0)$ molecules were excited by an infinitely short pulse of light, then the number of molecules in the excited state can be described as a function of time by the following rate equation, where Γ is their radiative decay rate and k_{nr} is the nonradiative decay rate:

$$\frac{dN(t)}{dt} = -(\Gamma + k_{nr})N(t) \tag{2}$$

The solution of equation (2) describes the evolution (decay) of excited molecule populations in the absence of illumination and represents fluorescence intensity decay, which for a single exponential is:

$$N(t) = N_0 e^{-t(\Gamma + k_{nr})} = N_0 e^{-\frac{t}{\tau}} \tag{3}$$

Intensity decay is a statistical process, and molecules in an excited state can be found after times longer that the fluorescence lifetime, τ. The decay can also be multi-exponential in cases of complex structure of a molecule or simply because different types of molecules are present in the mixture.

$$N(t) = \sum_i N_{0i} e^{-t(\Gamma + k_{nr})_i} = \sum_i N_{0i} e^{-\frac{t}{\tau_i}} \tag{4}$$

Due to the high sensitivity of fluorescence lifetimes to the environment surrounding a fluorophore, fluorescence lifetime measurements have many practical applications, especially in biology [45,46].

Fluorescence Lifetime Measurements

Lifetime measurements require more advanced instrumentation than emission spectra measurements, as well as more complex software for collecting and analyzing data. The most popular types of fluorescence lifetime measurements are time domain, frequency domain, and streak camera measurements [46]. Herein I will only describe time domain measurements. [46, 47]

A sample is excited by an infinitely sharp pulse, which is considered to be a $\delta-$function. As a result, an initial excited state population is created (Figure 7). The number of excited molecules at subsequent times can be described by the exponential model described by equation (4).

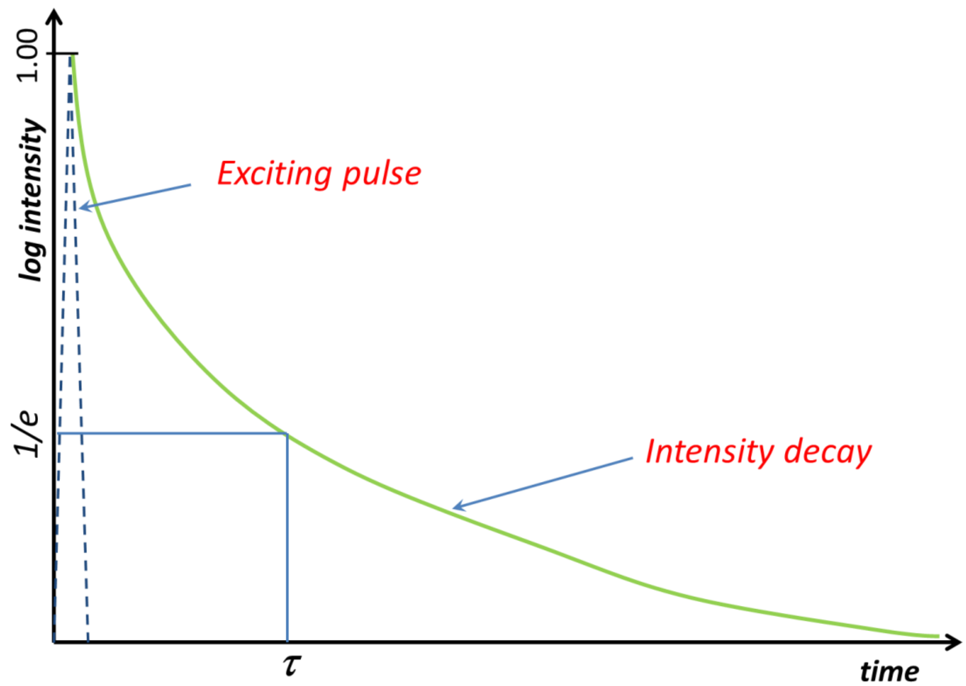

Figure 7. Simulation of fluorescence intensity decay

Since the experimentally available pulses are not infinitely short the analysis of intensity decay data is a complex procedure that involves deconvolution of the excitation pulse, instrument response and experimental model to the assumed decay.

Fluorescence lifetime measurements are typically performed in the same geometrical configuration as steady state measurements. A light beam is directed onto the sample at 90° to the detector to prevent excitation light leaking into it. An emission monochromator or a narrow bandpass filter is used for selection of the observation wavelength. An excitation monochromator or filters can also be used if the excitation source is a flashlamp or a multiwavelength pulsed light source, for instance, the super-continuum laser. Our laboratory is equipped with PicoQuant FT300, a fluorescence time-resolved spectrometer, based on Time Correlated Single Photon Counting (TCSPC) technique [47].

Time Correlated Single Photon Counting

Most modern time domain system measurements utilize the time-correlated single photon counting technique. I will outline the basic principles of TCSPC and describe various instrumentations used.

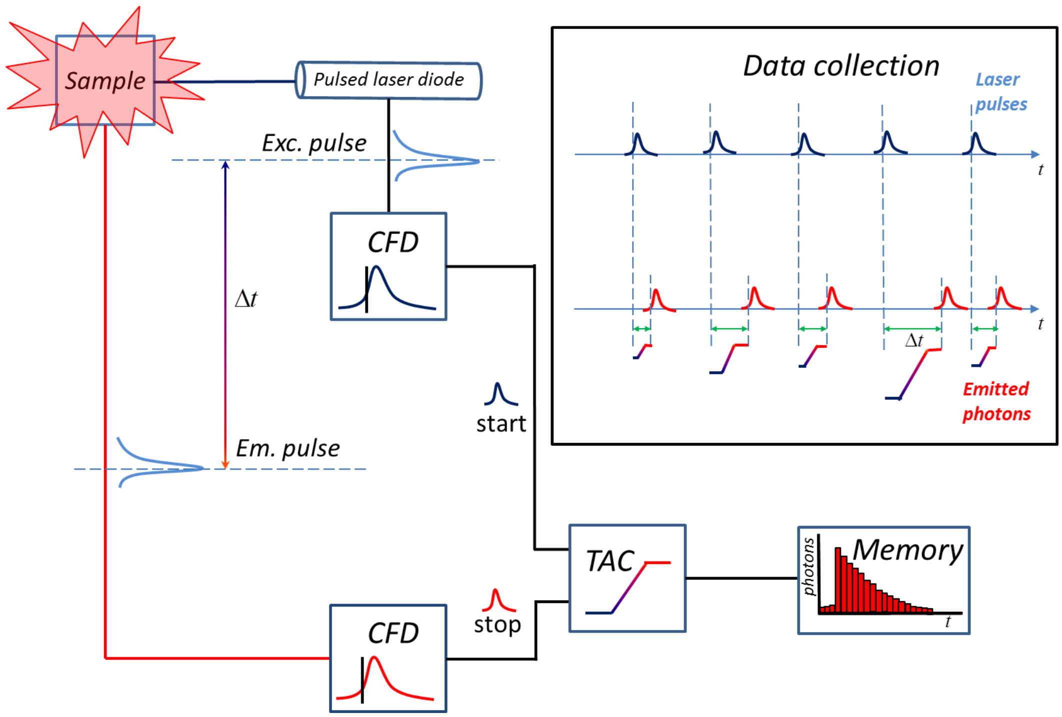

Figure 8. Time Correlated Single Photon Counting instrumental scheme

A sample is excited with a pulsed light source with constant repetition rate. The repetition rate is the frequency of the pulsing laser. The detection process is started with an excitation pulse that excites the sample and activates the electronics (Figure 8). The CFD, constant fraction discriminator, determines the time of the laser pulse arrival very precisely [47]. Start and stop pulses can have amplitude jitter that may cause time jitter in the order of the pulse's rise time. CFD's electronics are designed to eliminate these effects and determine accurate arrival time of the pulse. CFD also eliminates all possible background pulses produced in the detector, leaving only the signal. Then the TAC, time to amplitude converter, generates a voltage ramp that is stopped by another signal from the CFD, which is generated after the photon has arrived.

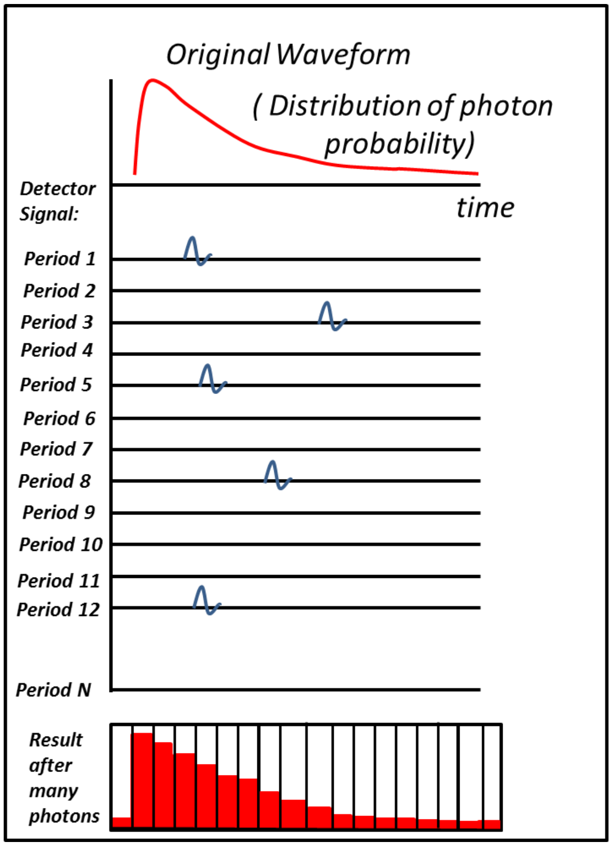

Figure 9. Distribution of the detected photons across the time channels

As a result, the TAC contains voltage that is proportional to the time between the initial and the detected pulse. The transformed TAC signal is stored in the address of the memory corresponding to the appropriate delay time. If no photon arrives, the cycle starts again with a new laser pulse. The time distribution of photon probability is displayed in the top part of Figure 9. Intensity of light is considered to be low enough so that the probability of detecting two or more photons in one signal period is negligibly small. The signal period is the time between exciting pulses. The detection rate usually varies from 0.1 to 0.01

photons per signal period. Higher detection rates cause shortening of the lifetimes since only the very first channel detects photons, and measurements will not provide the correct lifetime. Time scale is divided by the number of detector channels. When the measurement is completed, distribution of photons across the detector channels (bottom of Figure 9) is generated. [46,47,48].

TCSPC Data Analysis (Fitting)

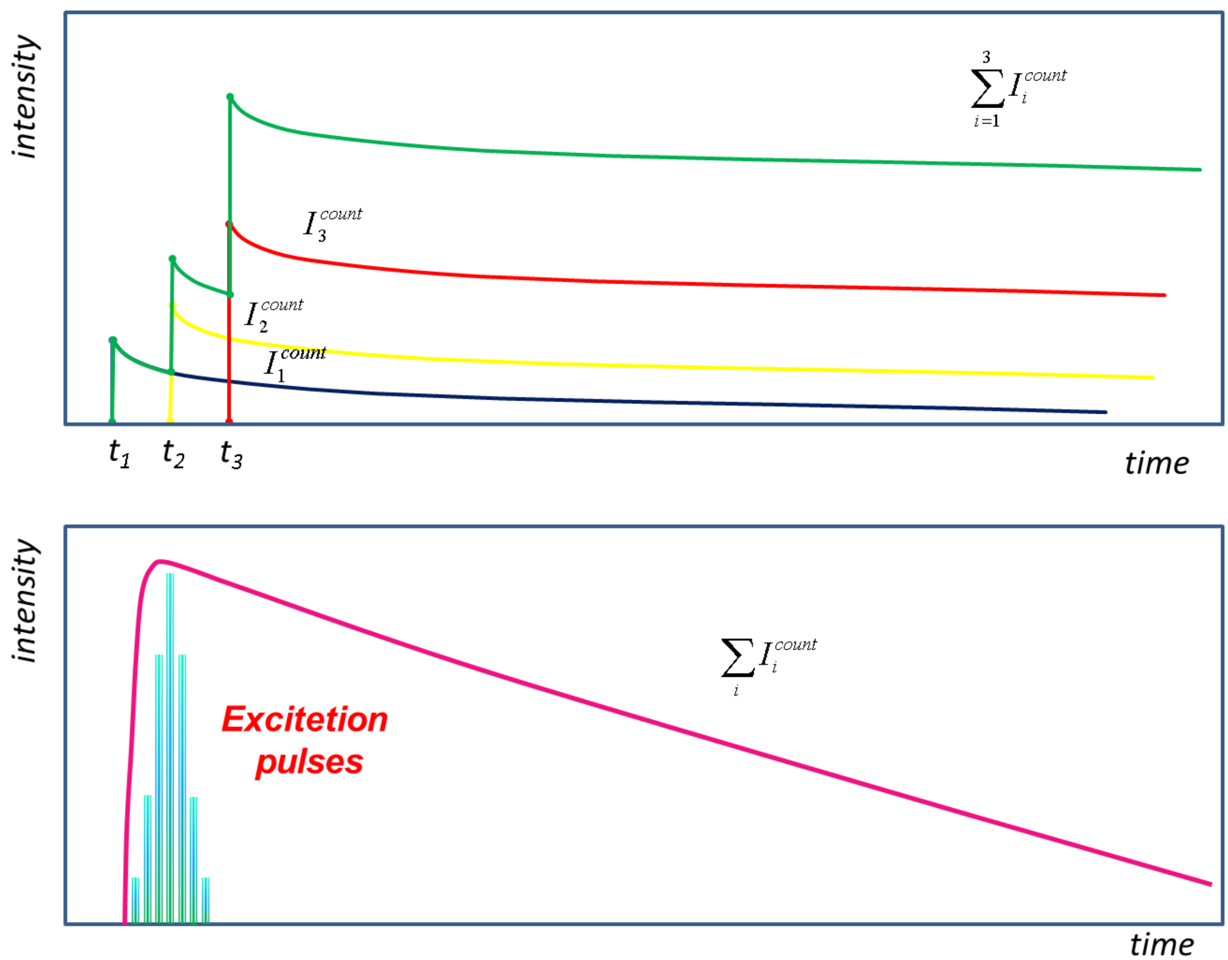

Figure 10. Convolution of lamp function response and decay

When the excitation pulse cannot be approximated by a delta function, the effect of signal broadening by the finite width of the pulse must be considered. Measured intensity decay is convoluted with the excitation source function, a “lamp function”. It is so called because it is impossible to measure the impulse response function directly. Most instruments have a response function approximately 0.05 – 2 ns broad. The excitation pulse can be interpreted as a series of δ - functions with different intensities (Figure 10). Each particular δ - function of the pulse excites an impulse response from the sample proportionally to its height. The intensity is proportional to the number of molecules in the excited state. Mathematically it can be expressed as:

$$I^{count}(t) = \int_0^{t_i} L(t) I(t_i - t) dt \tag{5}$$

where *L(t)* is the lamp function. The term *$(t_i – t)$* appears here because impulse response is started at $t = t_i$ and there are no molecules in the excited states before the excitation *$(t_i < t)$.* For convenience, equation (5) can be rewritten as [43,44]:

$$I^{count}(t_i) = \int_0^{t_i} L(t_i - t) I_0 e^{-t/\tau} dt \tag{6}$$

The measured signal is a convolution of the lamp function and the real intensity decay. The real intensity decay $I_0e^{-t/\tau}$ is obtained after deconvolution. Intensity decay represents the distribution of the photons' arrival time. An exponential function is typically used to fit obtained data. The total goodness of fit (χ^2) is expressed as a sum of corresponding variables:

$$\chi^2 = \sum_{i=1}^{n}\left[\frac{N^{ob}(t_i) - N^{cal}(t_i)}{\eta_i}\right]^2 \tag{7}$$

Where N^{ob} is the number of counts in a time channel, N^{cal} is corresponding value of the fitting function. Standard deviation (η_i) is considered to be proportional to the square root of the number of counts in a channel:

$$\chi^2 = \sum_{i=1}^{n}\left[\frac{N^{ob}(t_i) - N^{cal}(t_i)}{\sqrt{N^{ob}}(t_i)}\right]^2 \tag{8}$$

χ^2 depends on the number of data points, so it is not the best way to judge goodness of the fit. Most fitting software use reduced chi squared (χ_R^2), which represents standard weighted least squares for the set of experimental data points and is represented by:

$$\chi_R^2 = \frac{1}{n}\sum_{i=1}^{m}\chi_i^2 = \frac{1}{n}\sum_{i=1}^{m}\left[\frac{N^{ob}(t_i) - N^{cal}(t_i)}{\sqrt{N^{ob}}(t_i)}\right]^2 \tag{9}$$

where n is the number of data points minus the number of fitting parameters, and m is the number of data points. Usually chi squared number around 1 represents a good fit, and the lifetimes obtained from particular experiment are considered to be reliable. [48,49,50]

EXPERIMENTAL RESULTS

Absorption

Measurements of AO absorption at low concentrations were done using standard cuvettes of various thicknesses (5 cm, 1 cm and 0.5 mm). As was presented in my Master's thesis [34], absorption measurements were performed in standard cuvettes of different thicknesses. For high concentrations (more than 0.6M) "sandwiches" made of Menzel-Gläser (Gerhard Menzel GmbH, Braunschweig, Germany) microscopy slides were used.

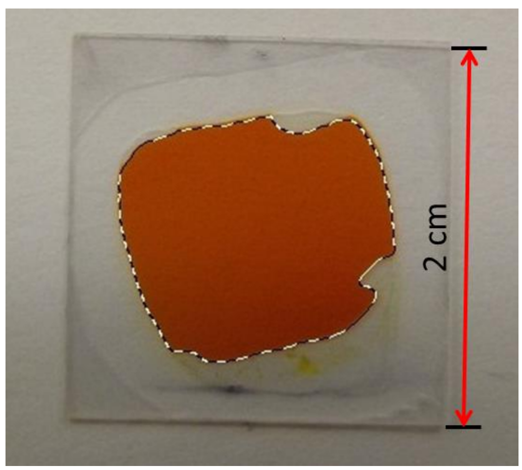

Figure 11. "Sandwich" prepared with Menzel-Gläser and markers

Sandwiches were prepared with markers for biological slides. For the highest concentrations close to the solubility limit (105 mM), the samples were squeezed without markers to limit the layer thickness to 1 – 2 microns. We have to stress that with such samples, slide deformation by surface tension often resulted in non-uniform layers, making control of actual thickness difficult. The normalized absorption spectra for various concentrations (10 M to 105 mM) are presented in Figure 12.

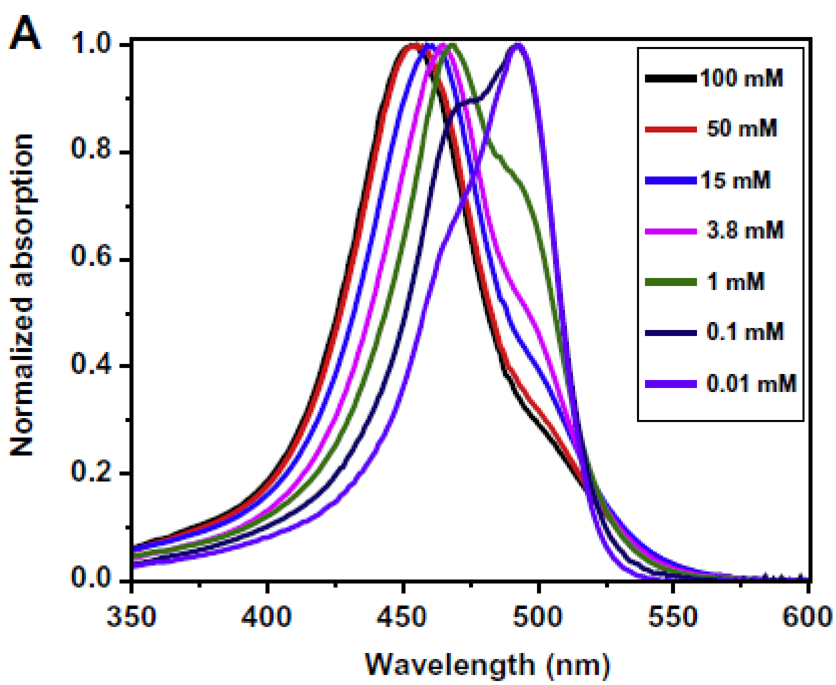

Figure 12. Absorption Spectra of Acridine Orange

Low concentrations of AO have absorption maximum around 494nm as was reported before [34]. Starting at 0.1 mM concentration, a short wavelength bump appears and it starts complete domination around 450 nm at concentration of 1mM and higher. Thus, excitation wavelength of excited monomers and dimers depends on the relative fraction.

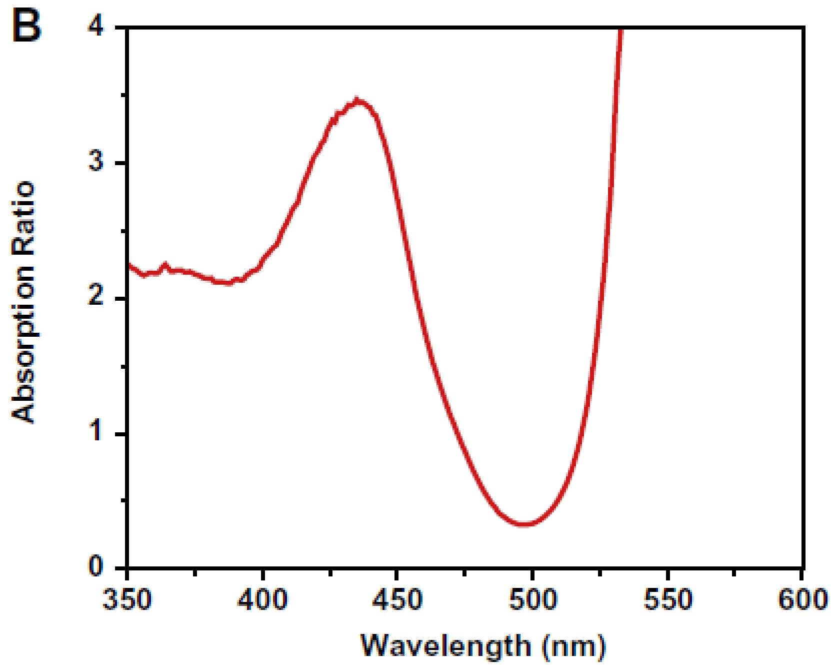

Figure 13. Ratio of absorption spectra for highest and lowest concentrations

Figure 13 represents ratio of absorption spectra of aggregates to monomers, which reveals a maximum at 435 nm and a minimum at 494 nm. It can be concluded that 435 nm excitation preferentially excites aggregates, while 494 nm excites monomers.

Emission

Low concentrations of Acridine Orange where monomers dominate can be measured in the square geometry with the help of standard cuvettes. For concentrations above 3 mM due to high absorption, a front-face configuration [34,51] must be used. Normalized emission spectra of AO at concentrations ranging from 10 nM to 100 mM in water excited at 494 nm and 435 nm are shown in Figure 14 and Figure 15 respectively.

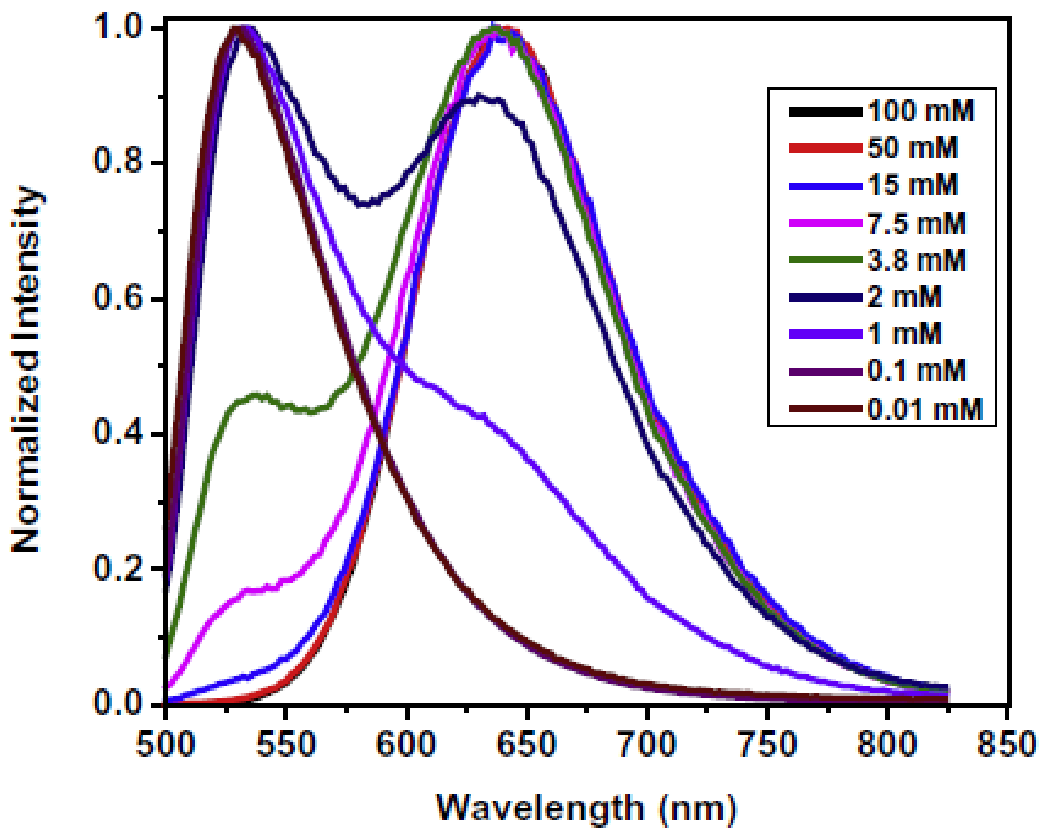

Figure 14. Normalized emission spectra of Acridine Orange with 435 nm excitation wavelength

Monomeric form is present at low concentrations and emits preferentially at 525 nm, while highest concentrations that contain mostly aggregates emit around 640 nm. The quantum yield measurements of the monomeric form were performed with the use of fluorescein (pH 9) as a reference dye, because it has emission maximum at around the same wavelength as monomeric form of the

AO. Quantum yield was calculated to be 0.155 ± 0.003. Detailed description of a quantum yield measurements can be found in my Master's thesis.

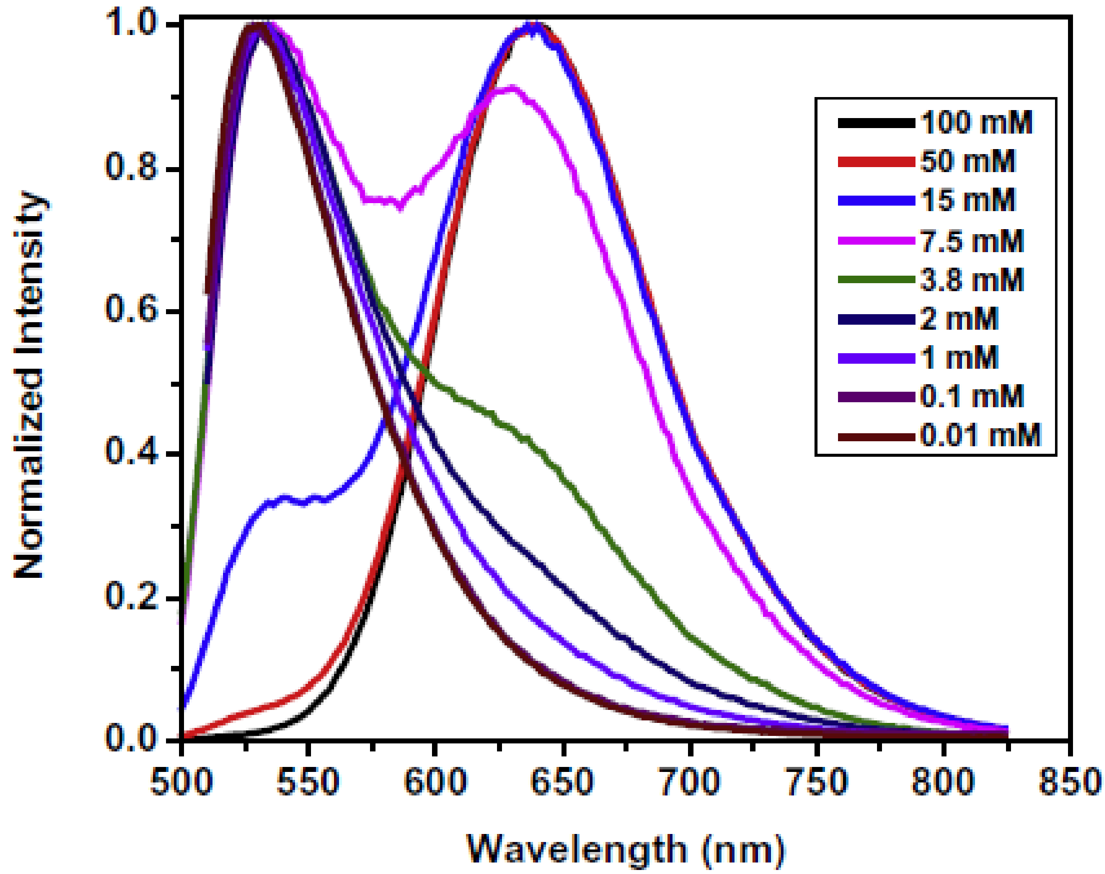

Figure 15. Normalized emission spectra of Acridine Orange with 494 nm excitation wavelength

Quantum yield of aggregates with concentration of 100mM was measured against a high concentration of Ruthenium dissolved in water as a reference dye. It was found to be 0.015 ± 0.002. Emission spectra of the highest concentration of

AO as well as lowest concentration do not depend on the excitation wavelength; this certifies that at low or high concentrations only a single fluorescent specie is present in the solution. The emission spectra of intermediate concentrations which contain both forms of AO is strongly dependent on the excitation wavelength, since it contains both forms of AO. As predicted from absorption spectra shown in Figure 13, excitation at 435 nm preferentially excites the aggregated form while 494 nm preferentially excites the monomeric form. These excitation wavelength can be obtained from the ratio of absorption spectra of aggregates and monomers (very high and very low concentrations of the AO). As an example of this, emission spectra measured for the two excitation wavelengths with 2 mM and 7.5 mM AO are shown in Figure 16 and Figure 17 respectively.

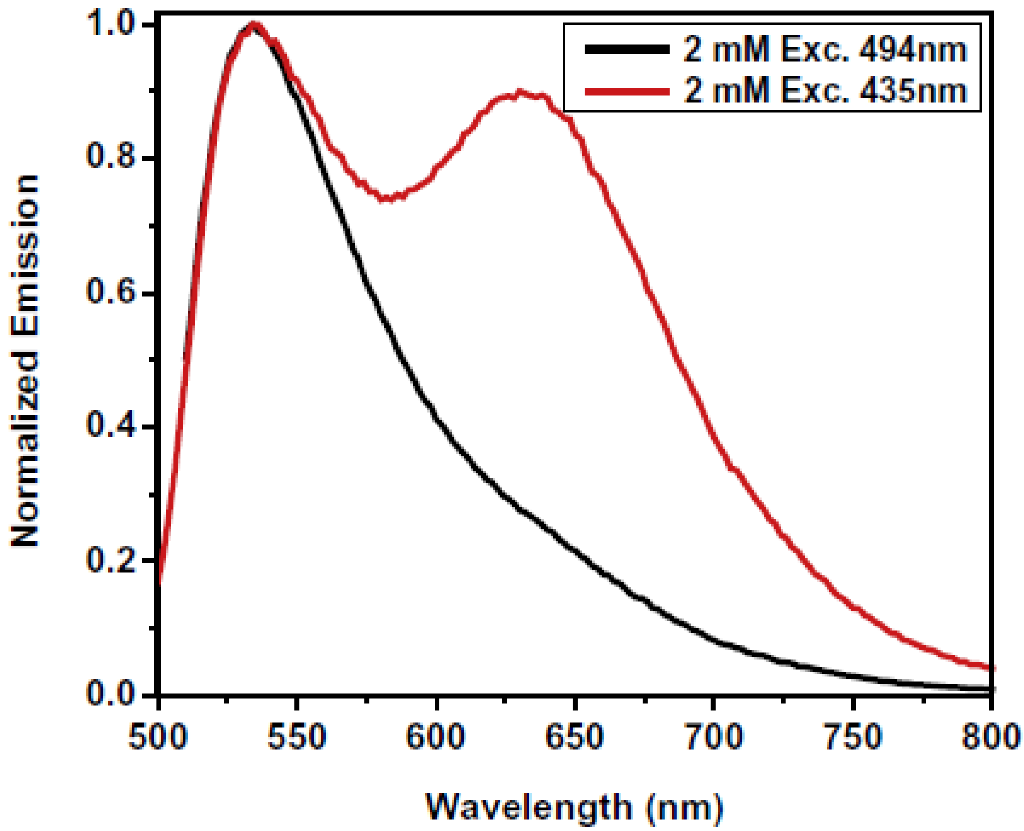

Figure 16. Normalized emission spectra of Acridine Orange at 2mM concentration with 494 nm excitation and 435 nm excitation wavelength

For the concentration of 2 mM excitation at 494 nm reveals almost pure monomeric form while for 7.5 mM concentration of 7.5 mM and excitation of 435 nm the emission is dominated by aggregates.

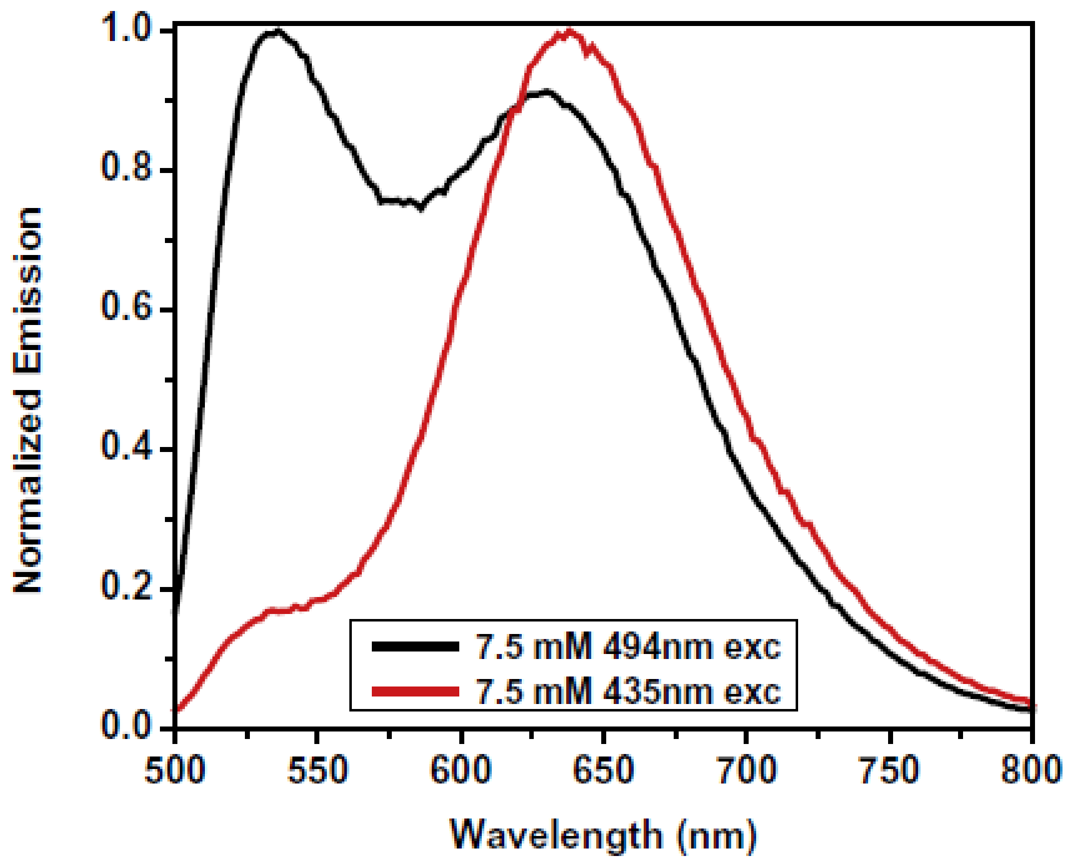

Figure 17. Normalized emission spectra of Acridine Orange at 7.5 mM concentration with 494 nm excitation and 435 nm excitation wavelength

The ability to preferentially excite one of the AO forms offers an opportunity for selective imaging of monomeric or aggregated forms over very broad concentration ranges simply by changing the excitation wavelength.

It is well known that AO accumulates in acidic intracellular compartments (pH 4.5 – 6.0) and shows significant spectral shift due to its aggregation [34, 40, 51]. To verify whether pH itself affects spectral properties of AO independently of its concentration we have measured emission spectra for the AO solutions of intermediate concentration of 4 mM and pH of 5.5 and 7.4, Figure 18.

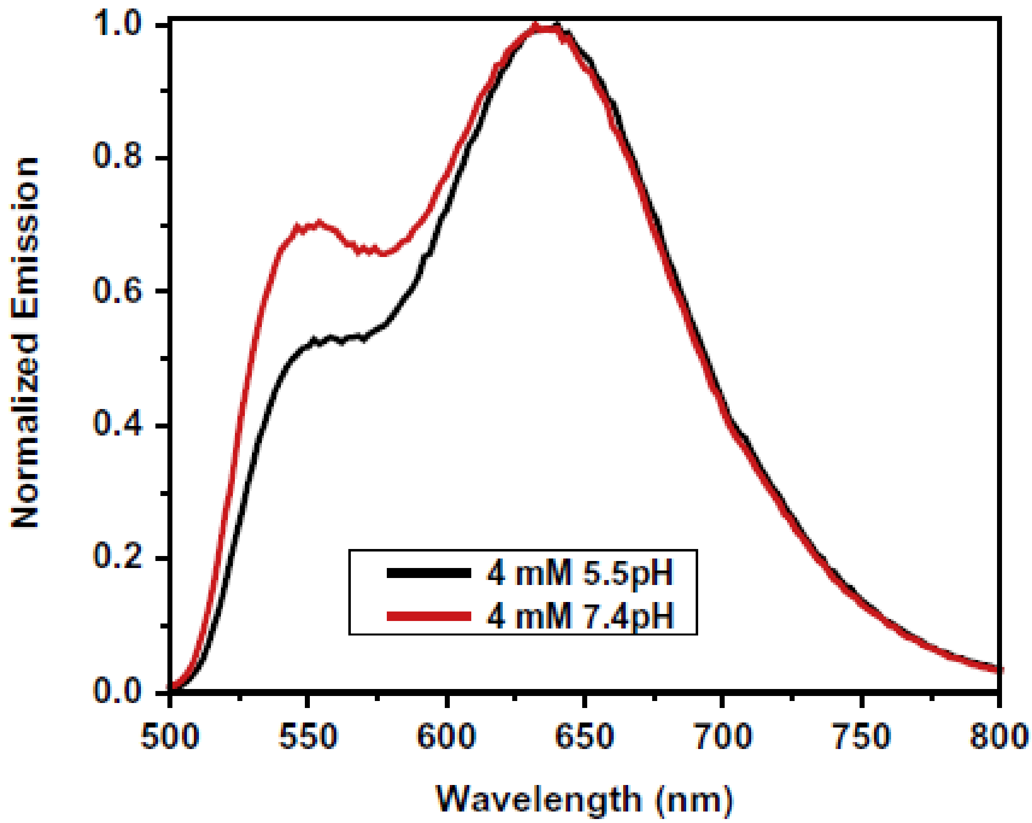

Figure 18. Normalized emission spectra for Acridine Orange at 3.8 mM concentration measured at pH 5.5 and pH 7.4 with 470 nm excitation

With 470 nm excitation, the emission spectrum shows somewhat higher content of dimer aggregates at lower pH, but a shift of almost 2 pH units had no big effect on the emission spectra that clearly can be attributed to slightly shifted equilibrium between monomers and aggregates. Time resolved intensity decays measurements were performed for various concentrations of AO. We have analyzed time-resolved emission intensity decays for AO concentrations ranging from a few nM up to a saturating concentration of 105 mM.

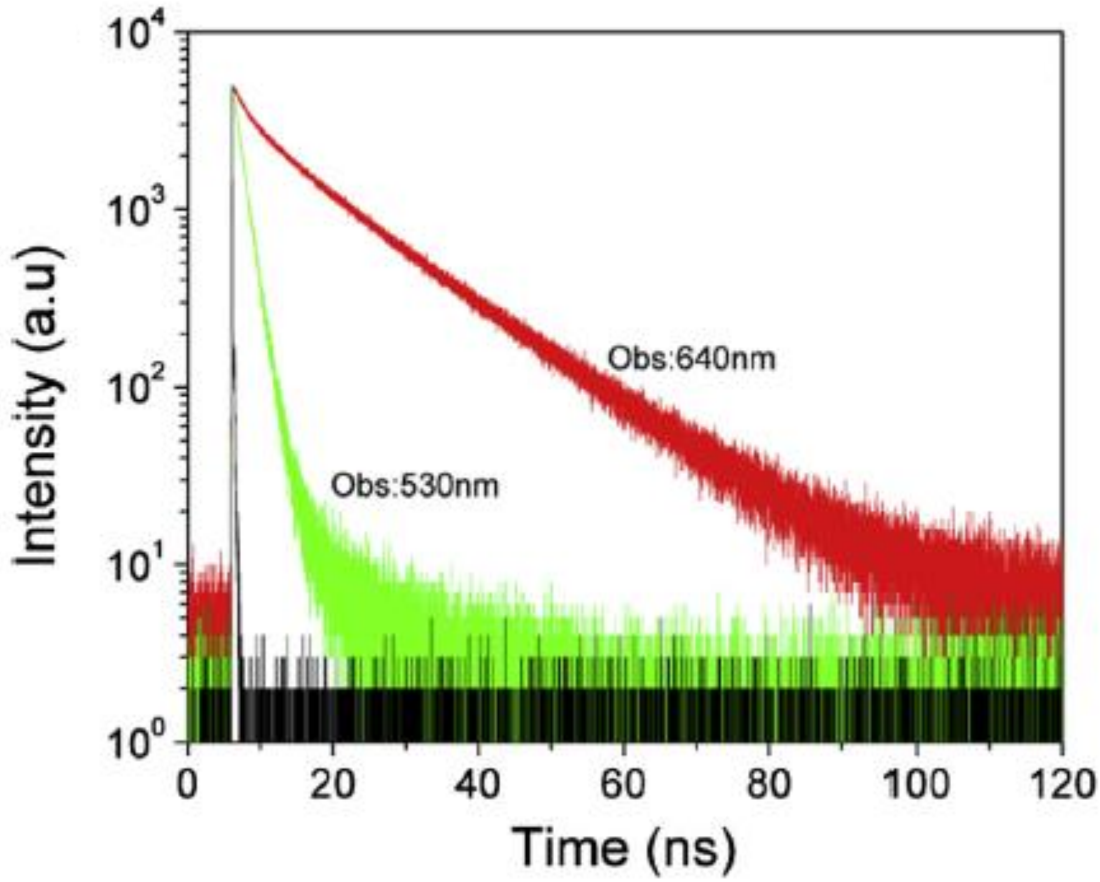

Figure 19. Example of fluorescence intensity decay of 3.8 mM Acridine Orange solution observed at 530 nm and 640 nm and excited with 435 nm

Two excitation wavelengths (that preferentially excite aggregated and monomeric forms respectively) 435 nm and 494 nm were used. Emission was observed at the corresponding peaks of the two forms 640 nm and 530 nm respectively. Examples of intensity decays for a concentration of 3.8 mM with 435 nm and 494 nm excitations are shown in Figure 19 and 20 respectively.

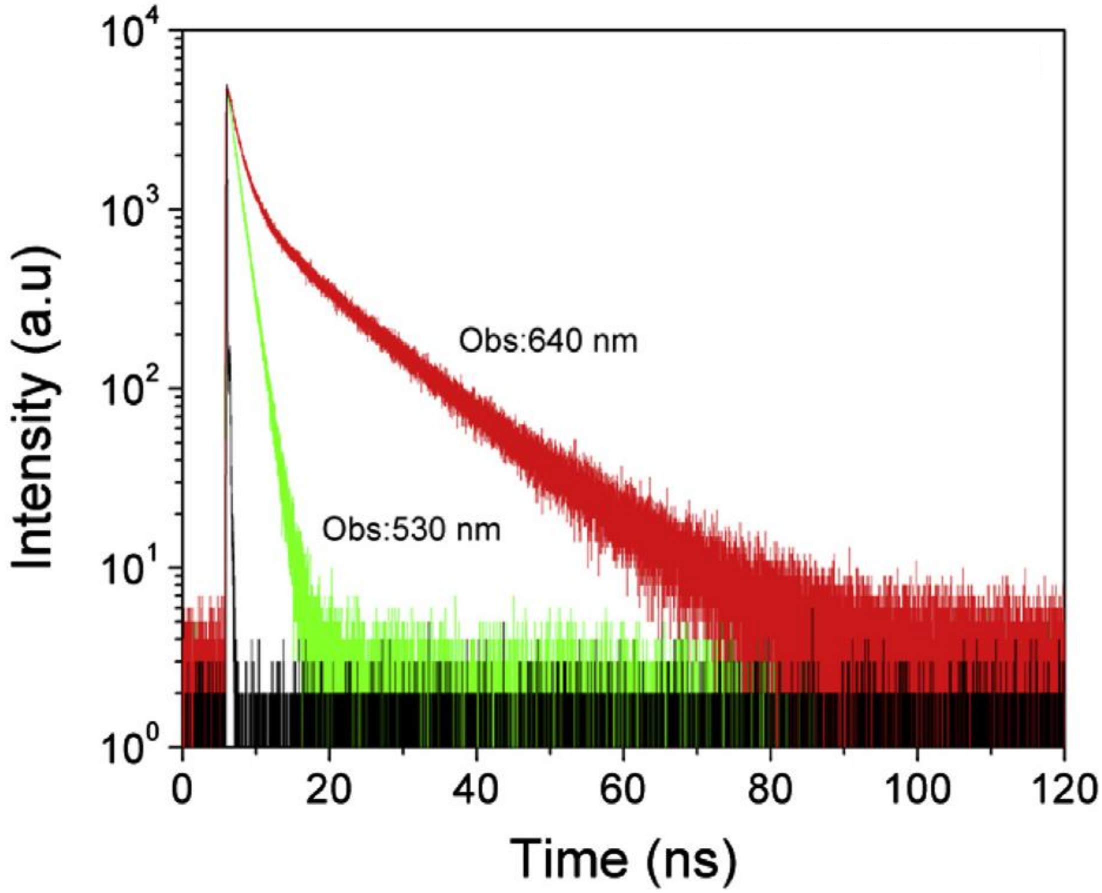

Figure 20. Example of fluorescence intensity decay of 3.8 mM Acridine Orange solution observed at 530 nm and 640 nm and excited with 494 nm

For this concentration we can observe a short time resolved intensity decay characteristic of a monomer, or a long time resolved intensity decay characteristic of an aggregated form.

Wavelength	*Concentration (mM)*	τ_1 *(ns)*	τ_2 *(ns)*	τ_3 *(ns)*	α_1	α_2	α_3	τ	$\langle\tau\rangle$
Exc = 494 nm	<0.2	1.75	-	-	1	-	-	1.75	1.75
Obs = 530 nm	3.8	2.431	1.547	0.504	0.07	0.905	0.025	1.53	1.48
	15	6.542	1.251	0.396	0.011	0.906	0.083	1.23	1.07
	52	12.881	0.873	0.302	0.094	0.674	0.232	1.87	0.65
	105	18.118	1.204	0.313	0.363	0.103	0.534	6.87	0.54
Exc=494 nm	<0.2	1.76	-	-	1	-	-	1.76	1.76
Obs=640 nm	3.8	13.914	5.701	1.492	0.541	0.166	0.293	8.9	3.8
	15	17.615	8.922	1.262	0.720	0.22	0.060	14.72	8.78
	52	20.603	8.305	1.004	0.87	0.11	0.02	18.86	13.72
	105	21.172	7.702	1.408	0.861	0.121	0.018	19.19	14.48
Exc = 435 nm	<0.2	1.779	0.219	-	0.989	0.011	-	1.76	1.64
Obs = 530 nm	3.8	2.434	1.567	0.476	0.026	0.938	0.036	1.64	1.47
	15	13.082	1.280	0.409	0.098	0.807	0.094	2.36	1.15
	52	18.089	1.076	0.360	0.497	0.307	0.196	9.38	1.16
	105	19.593	2.398	0.255	0.786	0.087	0.127	15.64	1.74
Exc = 435 nm	<0.04	1.78	-	-	1	-	-	1.78	1.78
Obs = 640 nm	0.2	5.721	1.831	-	0.077	0.923	-	2.64	2.13
	3.8	16.106	9.681	1.765	0.452	0.440	0.108	11.73	7.42
	15	18.571	10.837	1.546	0.680	0.294	0.026	15.86	12.43
	52	20.884	8.518	1.178	0.885	0.102	0.013	19.36	15.26
	105	21.029	6.534	1.230	0.89	0.098	0.012	19.36	14.81

Table 1. Recovered parameters for time – resolved intensity decays for 494 nm and 435 nm excitations and 640 nm and 530 nm observation wavelength

Table 1 shows details of decay parameters measured for various AO concentrations. Table1 demonstrates fitting parameters and characteristic lifetimes of the monomeric and aggregated forms of AO ($\tau_{1,}$ $\tau_{2,}$ τ_3 – lifetimes of 3 components presented in the decay, $\alpha_{1,}$ $\alpha_{2,}$ α_3 are fractional amplitudes, τ and $<\tau>$ are intensity and amplitude average lifetimes). Definitions and detailed description of these conventionally used parameters can be found in literature [45]. For low concentrations below 200 nM and excitation 494 nm (monomer peak absorption) a single intensity decay of 1.75 ns is observed at both 530 nm (monomer) and 640 nm (aggregate) emission wavelengths. Intensity decay collected with 435 nm (aggregate absorption band) excitation and 530 nm emission wavelengths is more complex, but average fluorescent lifetime is very close to the result obtained with 494 nm excitation. Observation at 640 nm (peak aggregate emission) clearly indicates the presence of a longer component already at 200 nM, but it is absent after 3 - 5 fold dilution producing a single exponential decay characteristic of monomeric form as presented in Table 1. Measurements performed at an emission wavelength of 640 nm indicate presence of longer component at 200 nM, but it is absent after 3 - 5 fold dilution and only the monomeric component of AO remains in the solution.

As the concentration of AO increases over 200 nM the intensity decays become more complex and fitting the data requires at least three components. Intensity decays of AO concentrations above 200 nM become more complex and require 3 components for a satisfactory fit. Lifetime measurements for a concentration of 3.8 mM with 435 nm excitation and 530 nm emission wavelength also become more complex, however there is no major change to the average lifetimes. Average fluorescence lifetimes start to slightly decrease at concentrations over 10 mM. This can only happen when the dominant emissive species (monomers in this case) are quenched, although we are not sure about the exact mechanism of such quenching. One possible explanation could be that aggregate formation is a dynamic process in which the aggregates have significantly lower quantum yield (as measured here about 10 - fold lower) and red-shifted emission. In this case excited monomers are depopulated by the formation of aggregates that have lower quantum yield and long decay component, so do not contribute to the intensity decay, especially at 530 nm emission wavelength. Interestingly this process appears at low centrations too, so there is the possibility of the formation of excited aggregates out of the monomers. Intensity decay of higher concentrations of AO collected with 435 nm excitation and 530 nm emission wavelengths has short components also.   In this case based on the absorption spectra, we expect that we preferentially excite aggregates. However, emission observed at 530 nm is probably the result of a dynamic dissociation process of aggregates since the intensity decay is very nonuniform and amplitude average lifetime appears to be shorter than that of a pure monomer. We want to stress that because the fluorescence lifetime of a monomer is short its diffusion is rather limited and the association of two excited monomers are negligible. Decrease of average fluorescence lifetimes is lower with 435 nm excitation because of aggregates' absorption, also aggregates' dissociation process and formation of monomers that contribute to the emission. For 494 nm excitation wavelength (monomer absorption) and 640 nm (aggregates emission) emission wavelength a significant long lifetime component can be observed with much longer average lifetimes already at low concentrations (mM range). For the concentration in the range of 3.8 mM, with 435 nm wavelength excitation shows very large change in fluorescence lifetimes indicating distinctive contribution of aggregate emission (Table 1 and Fig. 19 and 20). As AO concentrations increase above 3.8 mM longer fluorescence lifetimes become dominant reaching 20 ns for concentrations above 30 mM [34].

EXPERIMENTAL MOTIVATION

Mucosal exocytosis

Mucosal exocytosis is the process of release of a mucosal granule out of an epithelial cell and formation of the mucosal layer on the surface of the epithelial tissue. Cellular vesicles are formed in the Golgi apparatus.vThey are released out of the cells as a result of the exocytotic processes and contain granule that are represented by the densely packed mucins (Figure 21).

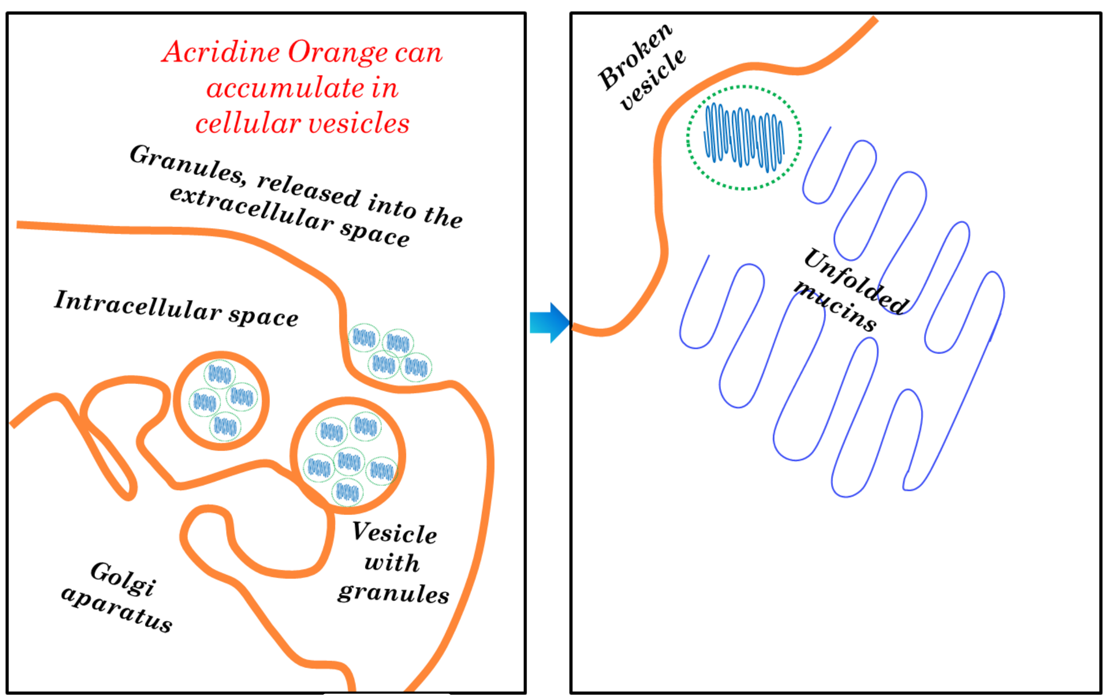

Figure 21. Schematic representation of the exocytotic process in Calu 3 cell.

Mucus plays an important role in the immune system. Mucus forms a uniform layer on the surface of epithelial tissue that traps external agents that may cause harm to the host organism (external pathogens like bacteria, viruses, dust particles, toxic compound). Mucus density differs depending on the epithelial tissue. The stomach mucus layer is much thicker than the lung mucus layer. For example, mucus ranges in thickness from 10 μm in the eye and trachea to 300 μm in the stomach and 700 μm in the intestine [35, 36]. Mucus formation and proper functionality is very important for protection of the host organism from the severe conditions of the environment. [52]

The epithelial tissue forms a layer between viscous mucosal layer and the organs of the host organism. These cells together with underlying leucocytes produce a huge variety of defensive compounds into the extracellular space that interact with the mucosal layer. These defensive compounds are very important in the mucosal layer, because epithelial cells on human organs, especially the lungs are facing a huge amount of aggressive external environment. To perform their respiratory function, the lungs require a not very thick and viscous mucus, that provides protection to the epithelial layer and organs. Mucus in living organisms also performs lubrication of the epithelial tissue. Trapped bacteria are killed by antibodies and bacteriophages that are present in mucus [31, 32,52]

COPD & CF

Chronic obstructive pulmonary disease and Cystic fibrosis impact large number of population. COPD is a major cause of disability, and it's the third leading cause of death in the United States. Currently, millions of people are diagnosed with COPD. Many more people may have the disease and not even know it.

COPD develops slowly. Symptoms often worsen over time and can limit your ability to do routine activities. Severe COPD may prevent you from doing even basic activities like walking, cooking, or taking care of yourself.

Most frequently COPD is diagnosted in middle – aged and older adults. There is no effective treatment for the COPD, but changes in the lifestyle and known medical treatments can increase an activity of individuals that are impacted by the COPD and decrease progress of the disease. Present studies dedicated to COPD as well as mucosal activities are mostly focused on the mucin structure, gel formation and mucosal clearance as a result of ciliar movement, but exocytotic process wasn't studied yet which can reveal an original problem of the disease [31, 32, 35].

The symptoms and severity of CF vary. If you or your child has the disease, you may have serious lung and digestive problems. If the disease is mild, symptoms may not show up until the teen or adult years [53, 54].

The symptoms and severity of CF also vary over time. Sometimes you'll have few symptoms. Other times, your symptoms may become more severe. As the disease gets worse, you'll have more severe symptoms more often.

Lung malfunction appears in early childhood in people that have CF. Accumulation of thick, sticky mucus on the lung epithelial tissue causes breathing problems and damages the lungs. Modern treatments can increase patient’s lifespan and quality of life, especially if the treatment was started in the childhood. There are complex programs that include treatment of the patient as well as physical exercise and respiratory therapies that can improve well-being of people suffering from the CF. All these methods are directed on the improvement of the individual’s general conditions, including respiratory function, but they do not provide possibility for an effective elimination of original source of the problem, only symptoms removal and decreasing damage to the lungs.

CF is a genetic disease in which malfunction of mucus secretion and formation can cause problematic clearance, especially in lung mucus. Study of the exocytotic process can have high scientific interest in this case too, as well as possible application in healthcare.

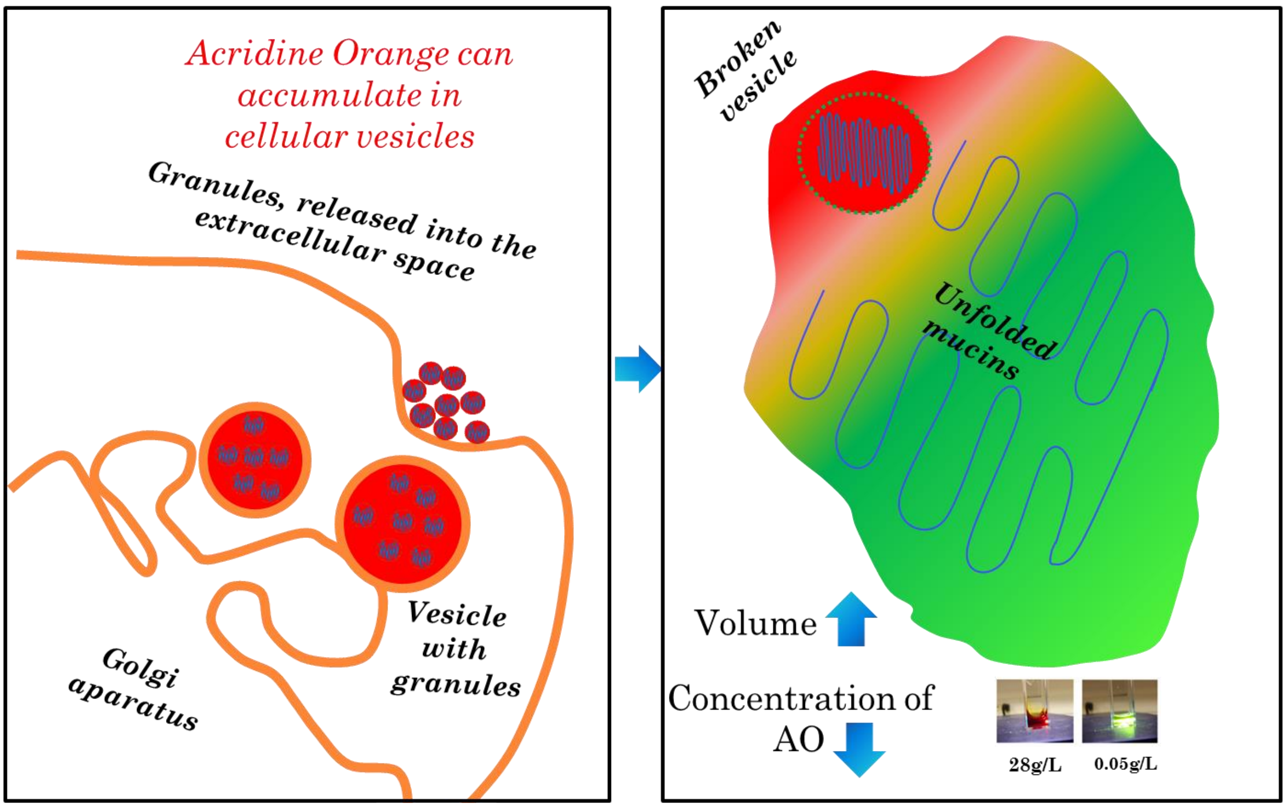

Figure 22. Schematic representation of the exocytotic process of the mucosal granulas that contain Acridine Orange.

As was discussed before Acridine Orange can accumulate in the cellular vesicles. When mucosal granules are released from the epithelial tissue mucins unfold in the extracellular space and increase in volume a few hundred times. Acridine Orange that is accumulated in the granules is released together with mucins and its concentration decreases (Figure 22). Change in concentration provides the possibility of monitoring the exocytotic process and comparing healthy Calu 3 cells and CF or COPD like cells [34, 53, 54].

EXPERIMENTS WITH MULTI - PULSE EXCITATION

Multipulse Approach

Multipulse excitation of fluorescent species was previously discussed for the imaging application where increase of signal to noise ratio is crucial [39]. Strong background signal is typically caused by Rayleigh and Raman scattering of the excitation light and intrinsic fluorescence of naturally occurring biological compounds. Gated detection may provide some improvement to the signal to background noise ratio, but overall signal from the system typically is not strong enough because long lifetime fluorophores have a low quantum yield. A gated detection approach and its advantages was briefly discussed earlier. Modern fluorescent dyes that can be excited in the visible range and have long lifetime that can be utilized with a gating technique typically have low extinction coefficients and low quantum yields that cause a low signal. Shifting of the excitation to the near infrared range (NIR) can cause a significant increase in the extinction coefficient, but this results in shortening of the fluorescence lifetime. Another method for eliminating background signal connected with autofluorescence in the cellular environment is to use a high concentration of the fluorescent dye. But this approach is not always applicable due to possible changes in cell's physiology (pH change, etc.).

We recently reported a method capable of enhancing selectively the signal-to-noise ratio with the use of long-lived fluorescent probes [39]. We used Ruthenium as a dye for the experiment in tissue imaging. Ruthenium lifetime is around 350 ns and the pulse burst of 10 or more pulses with an internal repetition rate of 80 MHz significantly increased the contribution of Ruthenium dye signal in comparison to a short lived tissue background. The very long fluorescence lifetime of Ruthenium was suitable for standard 80 MHz laser diode repetition rate where pulse-to-pulse separation is about 12.5 ns. During this time only a small fraction (~3%) of excited long-lived (350 ns) dyes will decay and each incoming pulse will add molecules to the existing population. However during 12.5 ns almost 50% of a dye with a 20 ns fluorescence lifetime will decay. To get a significant increase in population the pulse separation should be about 5-10 times lower than the fluorescence lifetime. For 20 ns this corresponds to about 2-4 ns separation between the pulses that requires a repetition rate of 250 – 500 MHz. Presently there are no available laser sources that can work at this repetition rate.

Multipulse excitation theory

Except in the single molecule detection experiments, many fluorescence based sensing/imaging experiments deal with a large number of molecules (number of molecules in one mole is $N_A = 6.02*10^{23}$ and millions of molecules are typically within the laser beam), but only a small fraction of molecules are excited. Even in fluorescent microscopy measurements, where very small confocal volumes are used only a few % of molecules can be excited.

Let's consider an excitation pulse that can be approximated by a delta function. It excites N_e molecules out of a total number of fluorescent molecules in the excitation volume N_T, with the condition that $N_T >> N_e$. After excitation, the number of molecules in the excited state decreases rapidly. Decrease of the number of molecules in the excited state can be described as:

$$N_e(t) = N_e e^{-t/\tau} \tag{10}$$

The number of emitted photons at any moment of time is proportional to the number of molecules in the excited state at a given time. Fluorescence intensity detected by the instrument is proportional to the total number of molecules in the excited state ($I(t) \sim N_e(t)$). For low repetition rates (RR), when the population of excited molecules decays completely before the arrival of the next pulse, the average steady-state intensity will be proportional just to the pulse intensity and the repetition rate of the laser, or in fact number of pulses per unit time. Repetition rates that are 80 MHz or lower give a pulse separation Δt > 12.5 ns. Most fluorophores decay within a few nanoseconds and molecules that have a fluorescence lifetime less than 4 ns excited by one pulse decays almost completely before the next pulse arrives. When the fluorescence lifetime is longer than the pulse separation (τ > Δt), the excited state population decays only partially and new molecules excited by the next incoming pulse are added to the molecules still in the excited state. In this case the number of molecules in the excited state will increase with each pulse reaching equilibrium when the number of molecules excited by a single pulse is equal to the number of molecules that return to the ground state over the time interval equal to the pulse separation, Δt. One can calculate the number of molecules in the excited state by analyzing subsequent excitations. The first pulse excites N_e molecules that, for simplicity, is much lower than total number of fluorophores in the excitation volume $N_e << N_0$. When the second pulse arrives, the number of molecules remaining in the excited state is $N_1 = N_e e^{-1/\tau \cdot RR}$ and the total number of excited molecules immediately after second pulse is: $N_e^1 = N_1 + N_e$ assuming that the second pulse excites the same number of molecules. In fact, the number of fluorophores available in the excitation volume is lower *(N_0 - N_1)*, but for our consideration we assume $N_0 \approx N_0 - N_1$. Extending this for *n* pulses, we have a geometrical series, and the number of molecules in the excited state after *n* pulses will be:

$$N_{eT}^{n} = N_e \frac{1-e^{-n/\tau \cdot RR}}{1-e^{-1/\tau \cdot RR}} \tag{11}$$

And consequently for an infinite number of pulses we have the semi-equilibrium condition where:

$$N_{eT} = \frac{N_e}{1-e^{-1/\tau \cdot RR}} \tag{12}$$

Clearly the total number of molecules in the excited state depends on the number of pulses and the repetition rate. As the number of pulses increases, the total number of molecules in the excited state increases asymptotically reaching equilibrium for a large number of pulses that only depends on fluorophore lifetime and the repetition rate.

Determination of the settings suitable for Acrdine Orange dilution detection with application of multiple pulses

In the previous chapters I described how Acridine Orange can be used to study exocytotic processes in cells. However extension of the detection range for dilution is limited by the low fluorescence intensity of aggregates. Since the aggregates have much longer fluorescence lifetimes we expect multiple pulse excitation to increase the population of excited aggregates. Aggregates are excited preferentially with 435 nm excitation and emit at 640 nm and have long lifetime of about 19 ns. At low concentrations monomers are mostly present in the solution. The absorption maximum for monomers is at 494 nm, but they can be also excited with 435 nm that is preferential for aggregates. Monomers have lifetimes of 1.7 ns. The excitation conditions should be adjusted to resolve differences between the lifetimes of aggregates and monomers with the greatest precision. Repetition rate of the "pulse burst" has to be selected as well as number of pulses in the burst that should be used for the experiment to achieve best resolution.

Number of molecules excited by the "pulse burst" can be calculated, using equation (11). Figure 23 represents the number of molecules in the excited state as a function of the number of pulses for fluorophores with different lifetimes ranging from 5 ns to 100 ns when excited with the source that allows 80 MHz RR in the burst.

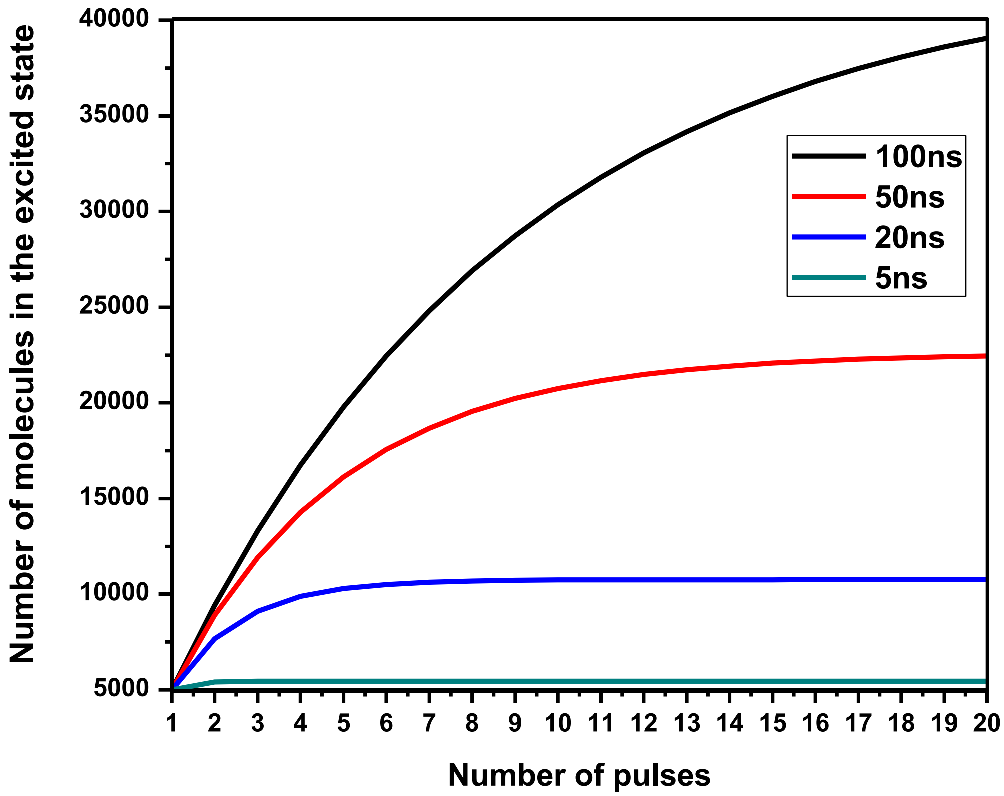

Figure 23. Number of molecules in the excited state as a function of the number of pulses with 80 MHz burst

It can be observed from the figure that number of molecules in the excited state with lifetimes of 20 ns and shorter practically does not depend on the number of pulses in the burst when more than 4 pulses are in the burst. For long lifetime fluorophores (50 ns and 100 ns), the number of excited molecules increases significantly. Dyes with lifetimes of 5 ns and less will not show significant increase of the number of molecules after 2 pulses.

We have already discussed that for shorter lifetimes the repetition rate in the burst that is needed should be much higher. Typically selected the RR should give separation about 5 times shorter than then the fluorescence lifetime. In the case of 20 ns we expect that a pulse separation of 3 ns, corresponding to RR = 330 MHz, will be sufficient.

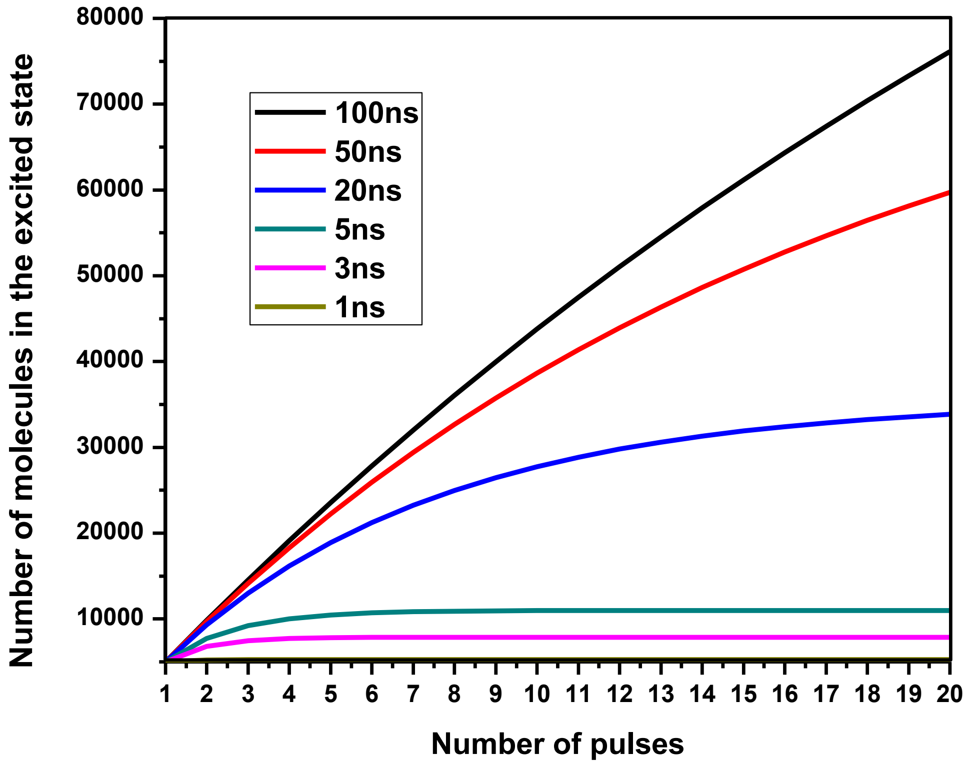

Figure 24. Number of molecules in the excited state as a function of the number of pulses with 330 MHz burst

Simulation performed with bursts of 330 MHz rate changes the picture dramatically (Figure 24). Separation between pulses in this case is around 3 ns. It is possible to see that number of molecules in the excited state of fluorophores with lifetimes of 100 ns, 50 ns and 20 ns grows dramatically, but for the fluorophores with lifetimes of 1, 3, 5 ns number of molecules in the excited state almost doesn’t increase.

Acridine Orange depending on concentration will present short (1.7 ns) or long (~20 ns) fluorescence lifetime. Using multipulse technology we want to increase long - lived population of excited aggregates as compare to short-lived monomers. This can be achieved when the excitation pulses in the burst has a repetition rate suitable to pump the dye with the longer lifetime and at the same time not to pump (or minimally pump) the dye with shorter lifetime. To determine the proper repetition we simulated the excited state population of the aggregates and monomers and consider a ratio of them as a function of the delay between pulses in the burst.

Figure 25 presents the relative ratio of number of molecules for different number of pulses as a function of pulse separation in the burst.

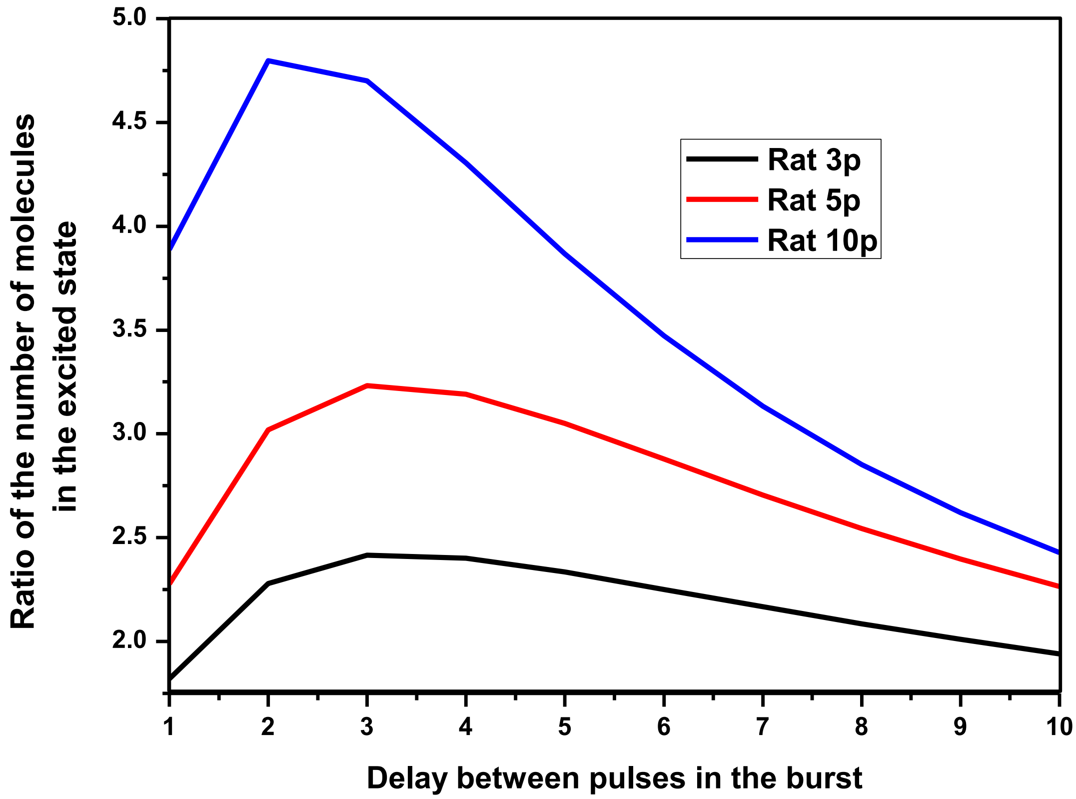

Figure 25. Ratio of the number of molecules excited by the burst of 5, 10 and 3 pulses respectively. Molecules have lifetime of 1.7 and 19 ns.

The blue curve represents ratio of molecules excited with 10 pulses, red curve with 5 pulses, and the green with 3 pulses in the burst respectively. From the plot it is possible to conclude that for our case the number of pulses in the burst should be 10 or more with the repetition rate of over 300 MHz to achieve best resolution. Unfortunately such high repetition rate cannot be obtained with present electronics and a standard repetition rate of 80 MHz does not produce a significant difference.

To study the AO system it is necessary to generate bursts of pulses with internal repetition rate higher than 300 MHz. To do this we engineered a special experimental set-up that allows splitting a single pulse to the desired number of pulses with fixed delay. Our goal is to test experimentally if such bursts improve detection resolution.

Experimental setup

The experimental setup has to be designed purpose to be able to produce "bursts of pulses" with constant time separation and constant repetition rate. The number of photons in the pulses (pulse intensity) should also be the same. The schematic of the generator is presented in Figure 26:

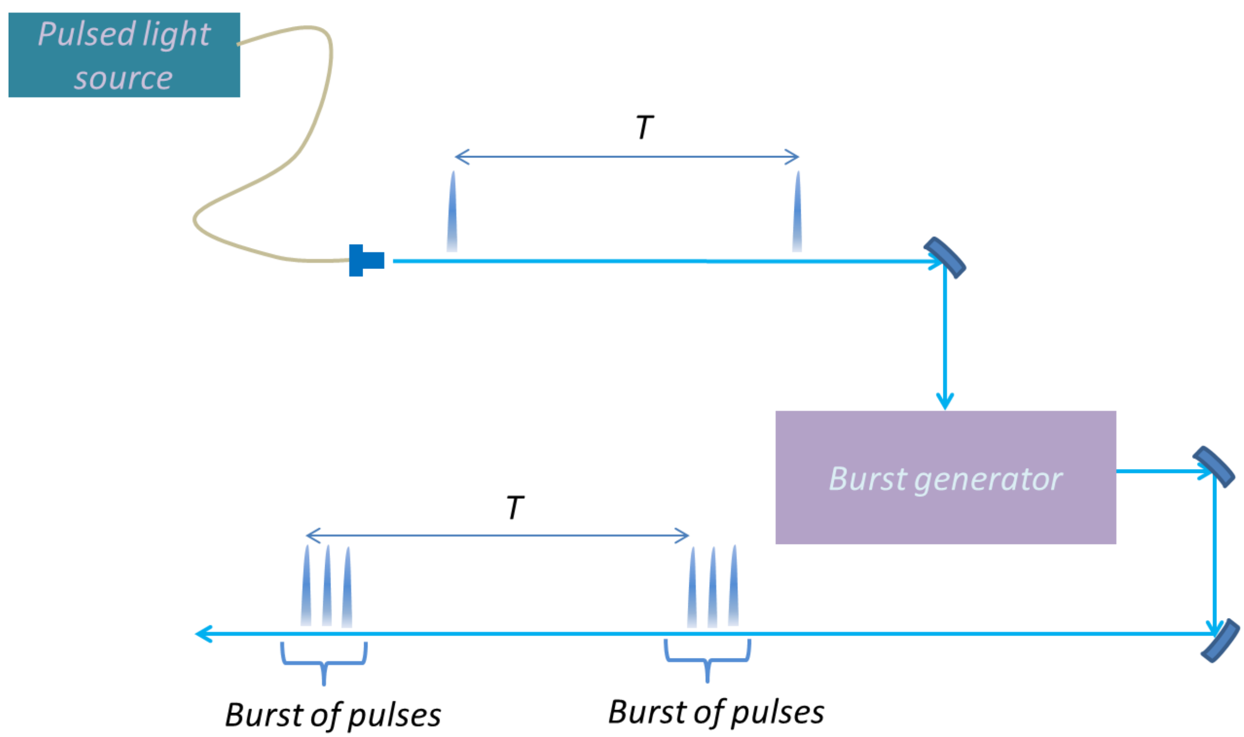

Figure 26. Schematic representation of the burst generator of in the multipulse experimental setup

One of the easiest and most effective ways to build a burst generator is to make a delay line with half transparent mirrors that will separate and combine pulses generated by a low repetition laser source. There are many low repetition laser sources available today.

A pulsed light source, typically a laser diode, generates pulses of a certain repetition rate. The repetition rate of the source is chosen to satisfy conditions of the particular measurement. Relatively short lifetimes (up to 2 ns) can be easily measured with the repetition rates of 80 MHz, because the full decay will fit into the distance between pulses. Longer lifetimes will require smaller repetition rates. Delays of a few nanoseconds may appear before the pulse due to configuration of the delay lines of the instrument. For long lifetimes of 20 ns the required repetition rate is not more than 5 MHz, because it will fit an entire intensity decay between pulses. To generate bursts we selected the RR of 5 MHz.

We used a supercontinuum laser system (Fianium) as a pulsed source connected with a monochromator to select the wavelength. An excitation wavelength of 435 nm that excites preferentially aggregates was selected. Measurements were performed using the FT 300 Fluorescent Lifetime Spectrometer in square geometry using 0.1 mm, 0.5 mm and 10 mm cuvettes for different concentrations of AO.

Development of the burst generator

A few commercially available systems, like MT 200 [55] can produce a burst of pulses with a maximum repetition of 80 MHz. This is sufficient for fluorescence lifetimes longer than 10 ns. There are a number of possibilities to build a generator for bursts of pulses of high repetition rate. As discussed earlier, pulses produced by the burst generator should have a constant repetition rate inside the burst as well as constant repetition rate between the bursts. The simplest approach will be to generate bursts from single low repetition pulses. Such low repetition pulses (below 80 MHz) are widely available from many commercial systems. The burst generator should produce the burst from each single pulse of the source. Dividing each original pulse from the generator into a few equal parts can be realized with partially reflective glasses/mirrors. For example a 45 degree thin glass will transmit about 90% of light intensity and reflect 10% under 90 degree angle. Using a set of a few glasses we can generate a few low intensity beams traveling perpendicular to the direction of original beam. We can sendl each beam on a trajectory that generates the desired delay. Typically a 30 cm difference in distance in air will generate a 1 ns delay. Recombining such beams into a single beam will create the burst of pulses of a given delay. After recombination bursts of pulses have the internal repetition rate required for the experiment and the burst repeats with the original repetition rate of the pulsed source.

The schematics for such design is presented on the Figure 26:

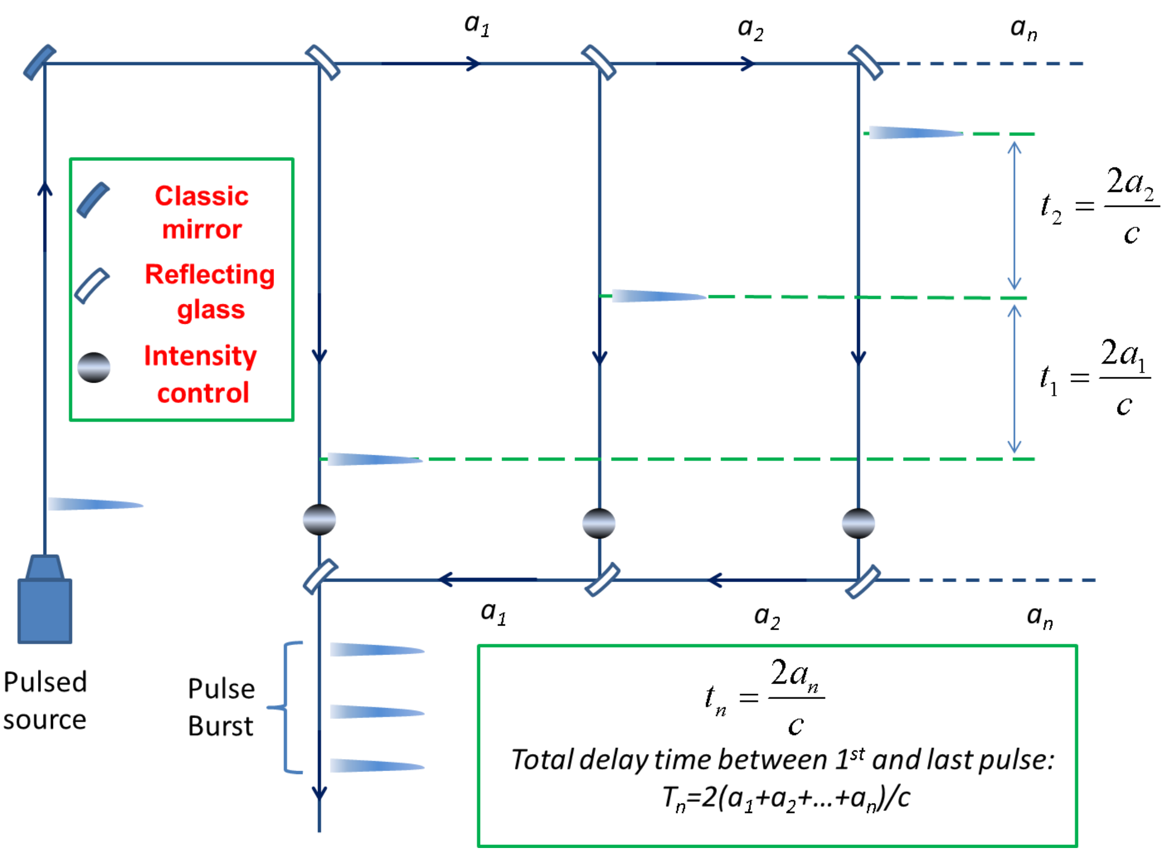

Figure 26. Schematic representation of the delay setup to produce burst of multiple pulses with help of delay lines

A pulsed laser source produces pulses of a certain repetition rate. Semitransparent mirror partially reflects incoming light and sends it to the sample. A second semitransparent mirror is placed at a distance *a* that sets the delay between pulses. Then it is possible to add any required number of semitransparent mirrors to split and combine the pulse. The number of mirrors will determine the number of pulses in the burst. It is obvious that the intensity of the beam after each reflection will be decreased, however todays laser sources typically have sufficient power. The delay between pulses is determined by the distance between mirrors *a* multiplied by two and divided by the speed of light, since light travels in both directions. In the ideal case,the intensity of light beam after combining back should be the same as it was before splitting. It is hard to achieve such result in real experimental conditions, but intensity of the each particular beam can be controlled with the help of neutral density filters that will limit/correct light intensity.

The setup that is used was prepared with help of Thorlabs M100 kinematic mirror mount and Menzel glasses. The distance *a* was chosen to be 0.45 m and two *a* equals 0.9 m. Since the speed of light c equals 3*10^8 m/s then the delay between pulses will be 3 ns or internal repetition rate of the burst will be 330 MHz. The photograph of the setup with schematics is represented on the Figure 27:

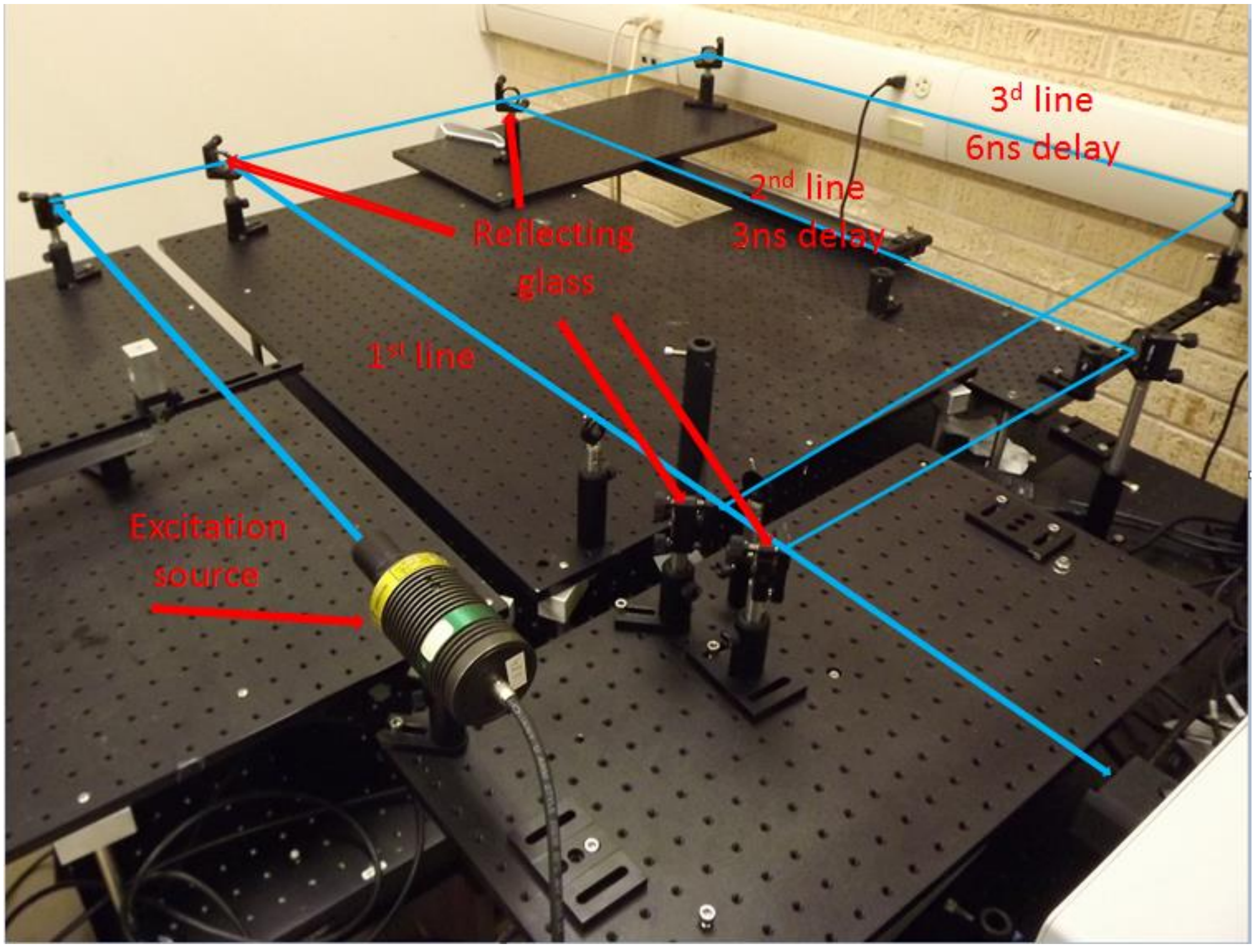

Figure 27. Photograph of the delay setup to produce burst of multiple pulses with help of delay lines

Fiber optics are widely used in the communication and laser technology. Optical fibers of a relatively small diameter can transfer up to 90% of the intensity that is produced by the source. Splitting of the fiber optics into a few channels with equal probability for each channel to obtain photons opens a possibility to select length of the fiber in each channel and control delay by the length of the fiber optics. Example of such a setup is presented in Figure 28:

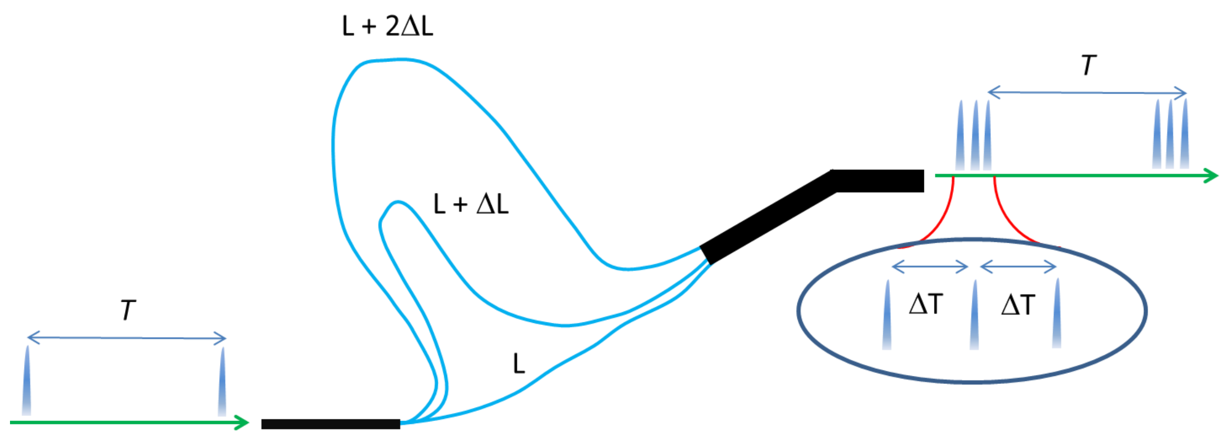

Figure 28. Schematic representation of the delay setup to produce burst of multiple pulses with help of fiber optics

Unfortunately this type of setup is hard to resolve as an engineering problem with our capabilities. Production of the fiber optics splitter requires precise machinery and equipment to produce precise splitter.

MULTI-PULSE EXCITATION EXPERIMENTAL RESULTS

Preliminary results of standards measurements

We decided to test the setup with measurements of mixtures of fluorophores with different fluorescence lifetimes. In such a way we can produce desired concentrations/fractions of different fluorescence lifetimes. Such systems will be important to test and calibrate measurements, since they will show the precision of our approach.

For preliminary lifetimes measurements we selected ADOTA and ErB (Erethrosine B) as dyes. ADOTA has a long average lifetime, around 20 ns and the ErB lifetime is short, around 0.5 ns. Measurements of such standards (known systems) will show how a short lifetime background can be eliminated in comparison to long lifetime fluorescent dyes. Measurements of Acridine Orange can be done in a similar way. First we measured instrument response function (IRF) using the 1st, 2nd and 3^{d} line. Two lines were blocked and only one was open. Then we measured the response function with all 3 lines open. Normalized spectra of the IRF are presented in Figure 29.

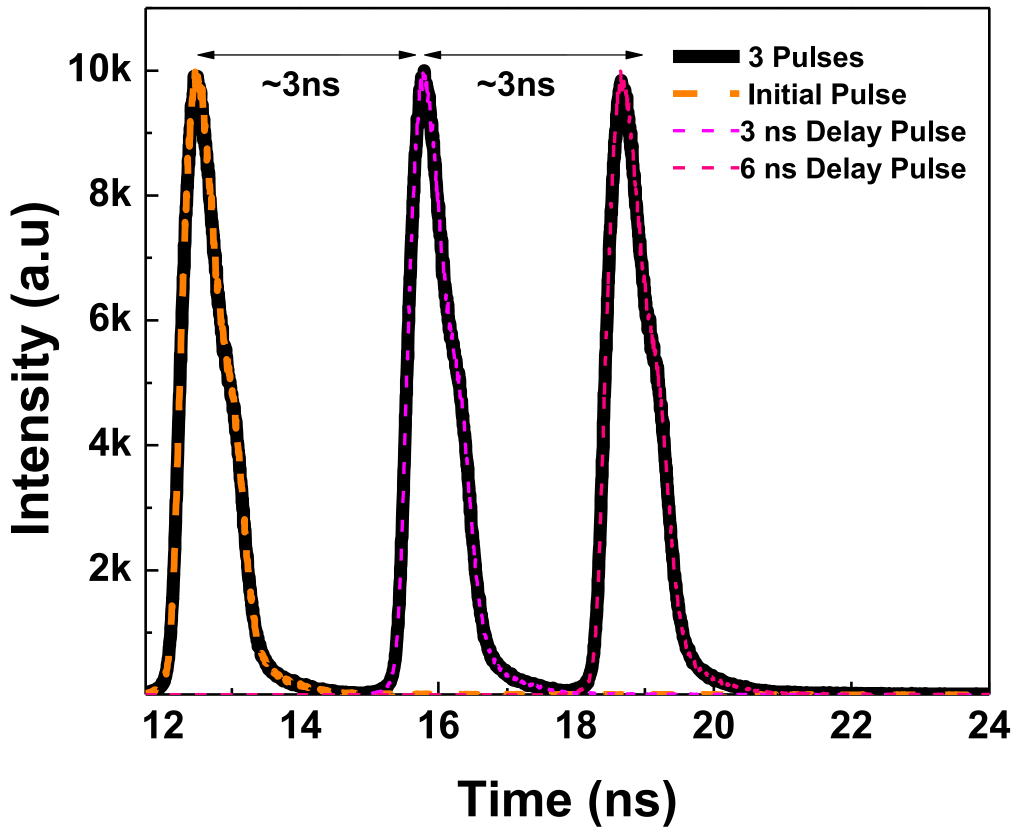

Figure 29. Instrument response function (IRF) that was generated with each delay line and all three lines together

Intensity decays of ErB and ADOTA also were measured with the use of single lines that produced pulses with an appropriate delay. Collected decays have the same lifetimes regardless of the initial delay of the pulse. Successive pulses excite almost exactly the same number of molecules. In the case of ErB, decay is almost finished before the next pulse arrives, so it is obvious that bursts of pulses will not be pumping molecules into the excited state. In the case of ADOTA, which has a 20 ns lifetime, the number of molecules in the excited state will be increased with each subsequent pulse in the burst.

Examples of the intensity decays of ADOTA and ErB are presented in Figure 30 and Figure 31.

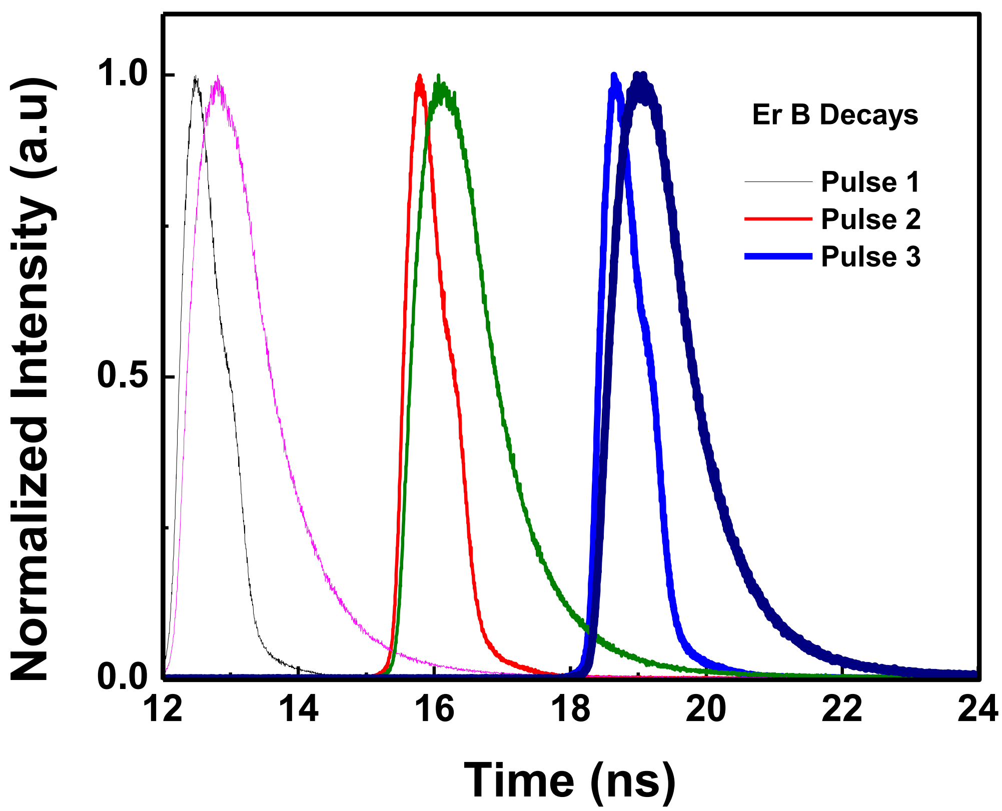

Figure 30. Intensity decay of ErB measured with single pulses generated by the delay lines

Plotted decays were collected separately and represent the number of molecules in the excited state after excitation with the burst of pulses. After excitation with the burst of pulses, the number of molecules in the excited state of each dye depends on its lifetime.

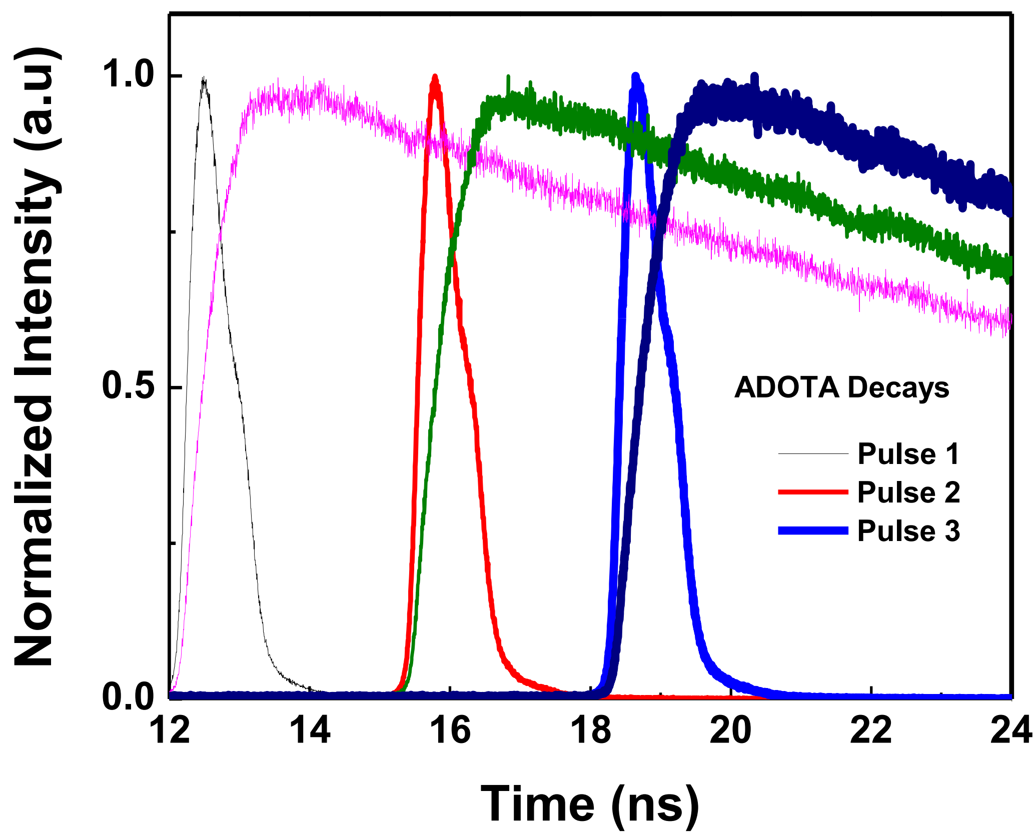

Figure 31. Intensity decay of ADOTA measured with single pulses generated by the delay lines

ErB will decay fast and the number of molecules in the excited state of this dye will not be increased significantly in comparison with the single pulse excitation, on the other hand, the number molecules in the excited state of ADOTA will show significant increase. This effect is demonstrated in Figure 32:

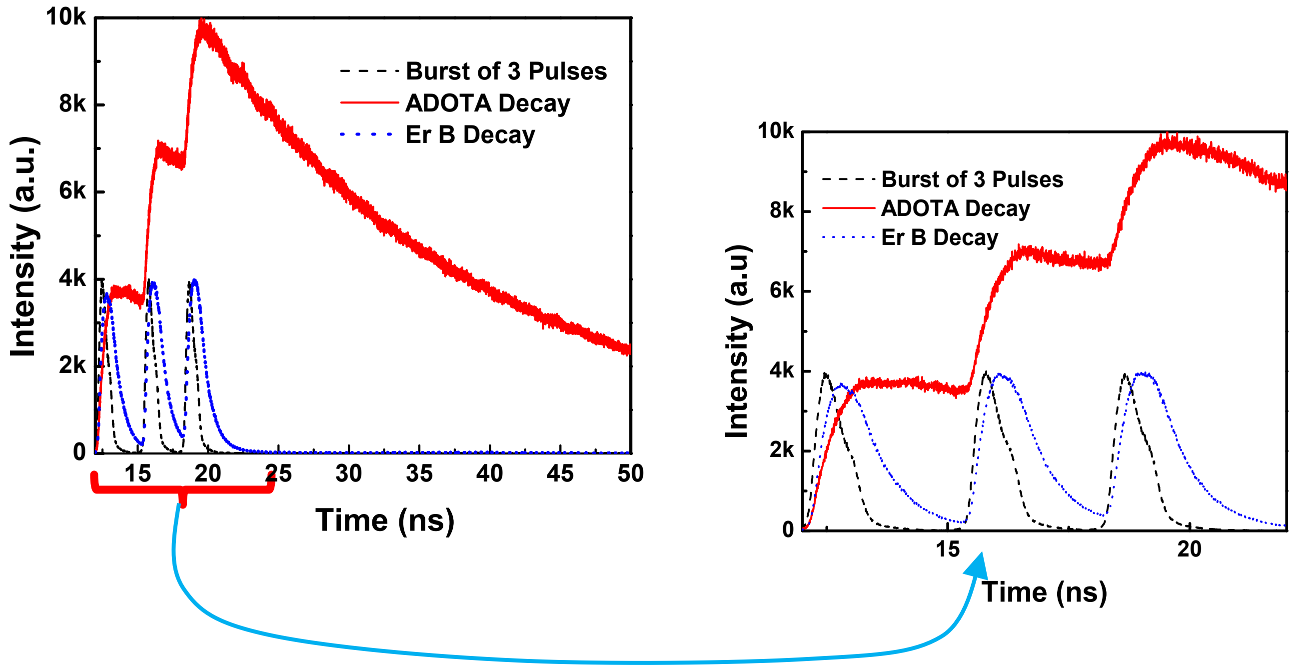

Figure 32. Intensity decay of mixture of ADOTA and ErB excited with the burst of 3 pulses and separation of 3 ns between pulses

These measurements clearly demonstrate the efficiency of multipulse excitation in order to increase signal to noise ratio in the system with different dyes that have short and long lifetimes. The number of excited molecules of the dye that has a longer lifetime will increase with the number of pulses; this does not happen to molecules of the short lifetime dye.

It can be concluded from our results that the scheme of multipulse excitation can be used for Acridine Orange measurements. At lower concentrations, AO will present short and long lifetime components that correspond to monomers and aggregates respectively. Successful application of the multipulse excitation using parameters that were described before can significantly increase the range and resolution of the mucus secretion measurements.

Measurements of Acridine Orange dilution with application of multiple pulse excitation

Concentrations of 1 mM, 0.4 mM, 0.2 mM, 0.1 mM, 0.02 mM were selected for the experiment. These concentrations were chosen because increase in sensitivity and resolution can be monitored in this range. Acridine Orange at a concentration of 15 mM accumulates in the cellular vesicles has dominant long lifetimes of the aggregates around 19 ns, but the monomeric form is also present at a low level. At a concentration around 2 mM L emission spectra show almost equal fractions emitted by aggregates and monomers. Concentrations of 1 mM already can be measured on the edge of the standard 0.1 cm cuvette. This concentration is high enough for good intensity counts and measurements of the emission spectra and was selected as an initial concentration. Further dilution causes rapid increase of monomers in the solution, while the fraction of the aggregates decreases.

Figure 33 shows intensity decay of Acridine Orangeat a concentration of 1 mM excited with a 435 nm single pulse. Also it shows fractional amplitudes and intensities of all the fluorescent species presented in the decay.

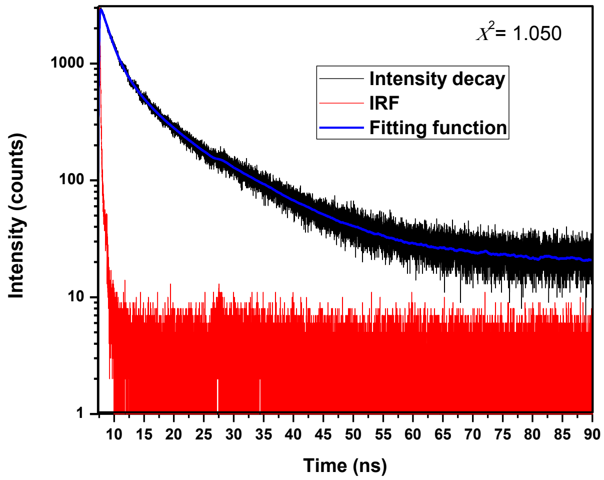

1 mM, 1 pulse

Intensity average lifetime:

τ_A =3.844 ns

Intensity average lifetime:

τ_I =8.043 ns

Parameter	Value	Conf. Lower	Conf. Upper	Conf. Estimation
A_1 [Cnts]	1078.9	-23.3	+23.3	Fitting
τ_1 [ns]	12.410	-0.194	+0.194	Fitting
A_2 [Cnts]	2064.4	-84.4	+84.4	Fitting
τ_2 [ns]	3.186	-0.121	+0.121	Fitting
A_3 [Cnts]	3071	-166	+166	Fitting
τ_3 [ns]	1.2768	-0.0755	+0.0755	Fitting
Bkgr. $_{Dec}$ [Cnts]	20.09	-1.07	+1.07	Fitting
Bkgr. $_{IRF}$ [Cnts]	2.30	-1.93	+1.93	Fitting
Shift $_{IRF}$ [ns]	-0.04134	-0.00965	+0.00965	Fitting

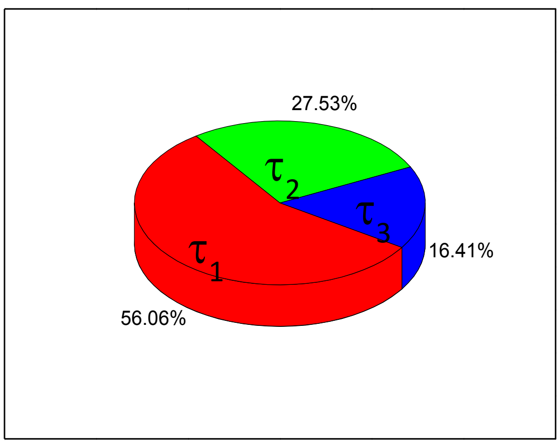

Fractional intensities of the Positive Decay Components

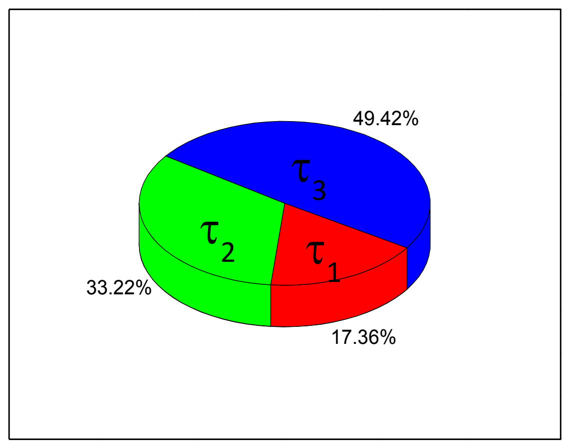

Fractional amplitudes of the Positive Decay Components

Figure 33. Intensity decay of Acridine Orange with the table of fitting parameters. Average intensity and amplitude lifetimes. Pie plots of the fractional intensities and amplitudes for concentration 1 mM, 1 pulse exc.

From Figure 33 it is easy to see that intensity decay contain a long component around 12.4 ns and two shorter 3.2 ns and 1.27 ns components. In fractional intensities decay, the long component dominates, but in the amplitude decays it has only small fraction, since the number of excited monomers is bigger at the moment.

Table below the intensity decay plot represents amplitudes and lifetimes of species presented in the decay. Amplitude average lifetime represent contribution of each specie to the total lifetime at t = 0. Intensity average lifetime represent contribution of each specie to the total lifetime through all the decay. These parameters can be used to monitor fractions of species that are present in the intensity decay.

Figure 34 represents intensity decay of Acridine Orange at a concentration of 1 mM excited with a 3 pulse excitation at 435 nm

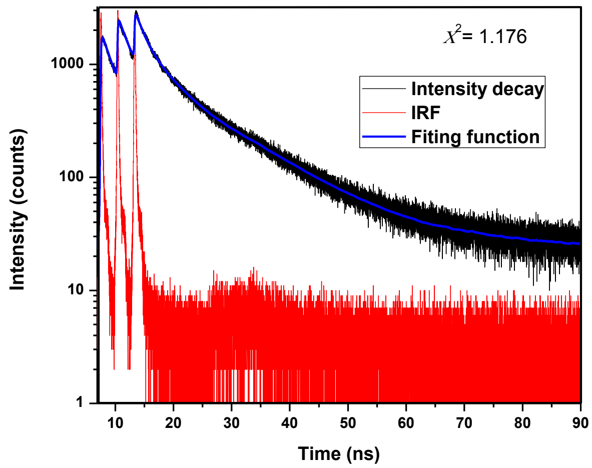

1 mM, 3 pulse

Amplitude average lifetime:
τ_A =3.832 ns

Intensity average lifetime:
τ_I =7.574 ns

Parameter	Value	Conf. $_{Lower}$	Conf. $_{Upper}$	Conf. $_{Estimation}$
A_1 [Cnts]	1689.0	-29.5	+29.5	Fitting
τ_1 [ns]	11.131	-0.135	+0.135	Fitting
A_2 [Cnts]	3315	-119	+119	Fitting
τ_2 [ns]	2.8324	-0.0658	+0.0658	Fitting
A_3 [Cnts]	3500	-271	+271	Fitting
τ_3 [ns]	1.043	-0.117	+0.117	Fitting
Bkgr. $_{Dec}$ [Cnts]	24.16	-1.34	+1.34	Fitting
Bkgr. $_{IRF}$ [Cnts]	3.086	-0.123	+0.123	Fitting
Shift $_{IRF}$ [ns]	-0.0377	-0.0104	+0.0104	Fitting

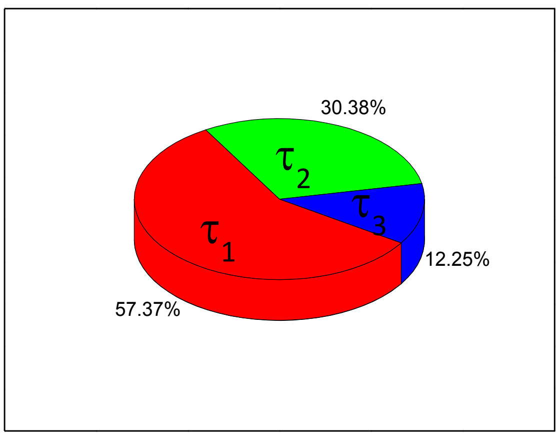

Fractional intensities of the Positive Decay Components

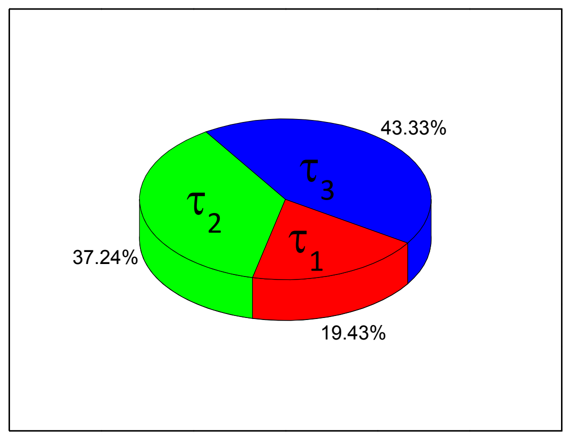

Fractional amplitudes of the Positive Decay Components

Figure 34. Intensity decay of Acridine Orange with the table of fitting parameters. Average intensity and amplitude lifetimes. Pie plots of the fractional intensities and amplitudes for concentration 1 mM, 3 pulse exc.

Excitation with 3 pulses causes a small increase of fractional intensity as well as increase in fractional amplitudes of the longest component, but the lifetime of the longest component is shorter than in the case of a single pulse excitation. Shortening of the lifetime of the longest component caused shortening in the average intensity weighted lifetimes and amplitude weighted lifetimes. We did expect certain interaction of the aggregates in the excited state or dissociation in the excited state that probably causes shortening of the lifetime of the aggregates.

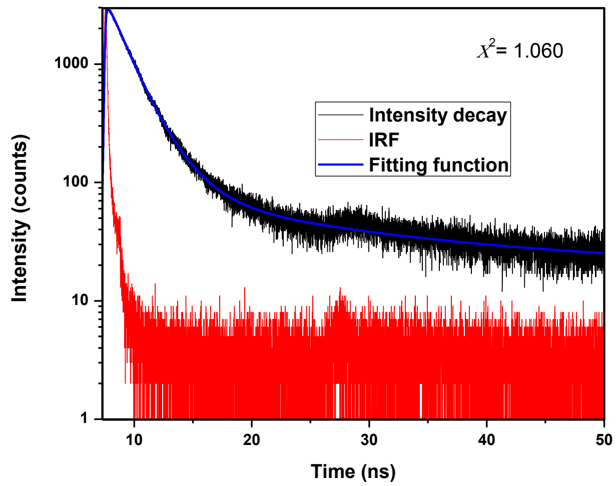

1 mM, 1 pulse

Amplitude average lifetime:

τ_A =2.02 ns

Intensity average lifetime:

τ_I =4.32ns

Parameter	Value	Conf. Lower	Conf. Upper	Conf. Estimation
A_1 [Cnts]	114.45	-6.73	+6.73	Fitting
τ_1 [ns]	17.54	-1.04	+1.04	Fitting
A_2 [Cnts]	4315	-109	+109	Fitting
τ_2 [ns]	1.3973	-0.0321	+0.0321	Fitting
A_3 [Cnts]	1956.6	-64.4	+64.4	Fitting
τ_3 [ns]	2.4734	-0.0617	+0.0617	Fitting
Bkgr. $_{Dec}$ [Cnts]	19.13	-1.07	+1.07	Fitting
Bkgr. $_{IRF}$ [Cnts]	1.13	-1.71	+1.71	Fitting
Shift $_{IRF}$ [ns]	-0.01697	-0.00707	+0.00707	Fitting
A $_{Scat}$ [Cnts]	15900	-11500	+11500	Fitting

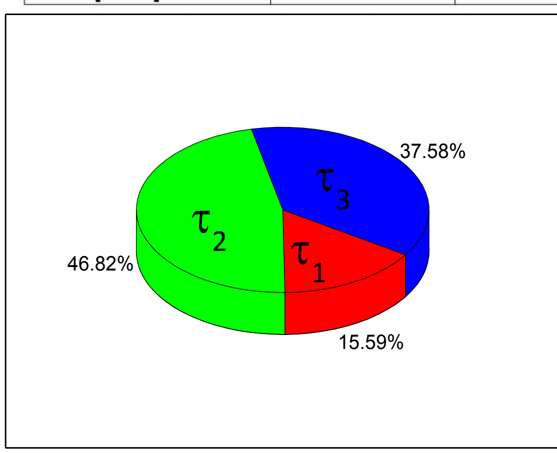

Fractional intensities of the Positive Decay Components

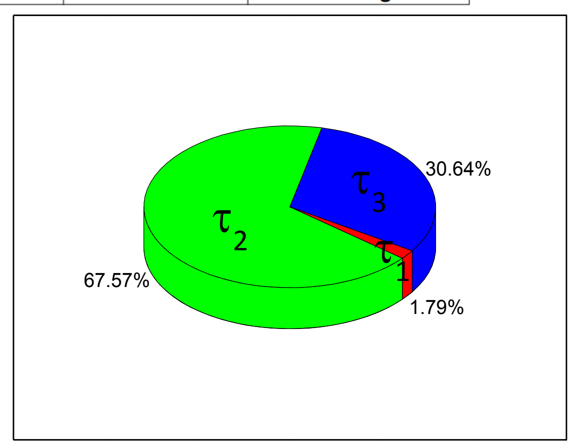

Fractional amplitudes of the Positive Decay Components

Figure 35. Intensity decay of the Acridine Orange with the table of fitting parameters. Average intensity and amplitude lifetimes. Pie plots of the fractional intensities and amplitudes for concentration 1 mM, 1 pulse exc.

Figure 35 shows the intensity decay of Acridine Orange with a concentration of 1 mM, excitation 435 nm, emission 640 nm. Excitation is conducted with asingle pulse. At this concentration, the number of aggregates in the excited state is much lower than the number of monomers. It is easy to see from the fractional amplitudes pie plot, where the fraction of the long component dye is not significant (around 2%). However in fractional intensities it is a little bigger because of the long lifetime. Intensity and amplitude weighted lifetimes in this case are lower.

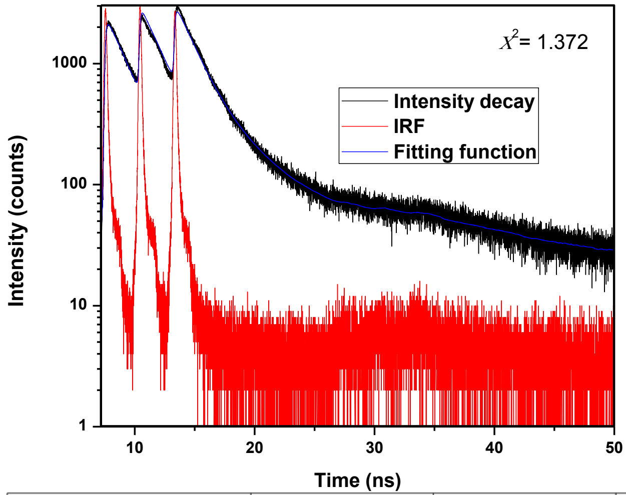

0.4 mM, 3 pulse

Amplitude average lifetime:

τ_A =1.944 ns

Intensity average lifetime:

τ_I =2.939 ns

Parameter	Value	Conf. $_{Lower}$	Conf. $_{Upper}$	Conf. $_{Estimation}$
A_1 [Cnts]	292.3	-22.2	+22.2	Fitting
τ_1 [ns]	9.505	-0.490	+0.490	Fitting
A_2 [Cnts]	3433	-112	+112	Fitting
τ_2 [ns]	2.4864	-0.0691	+0.0691	Fitting
A_3 [Cnts]	6709	-201	+201	Fitting
τ_3 [ns]	1.3374	-0.0383	+0.0383	Fitting
Bkgr. $_{Dec}$ [Cnts]	23.13	-1.49	+1.49	Fitting
Bkgr. $_{IRF}$ [Cnts]	3.500	-0.217	+0.217	Fitting
Shift $_{IRF}$ [ns]	-0.01503	-0.00906	+0.00906	Fitting

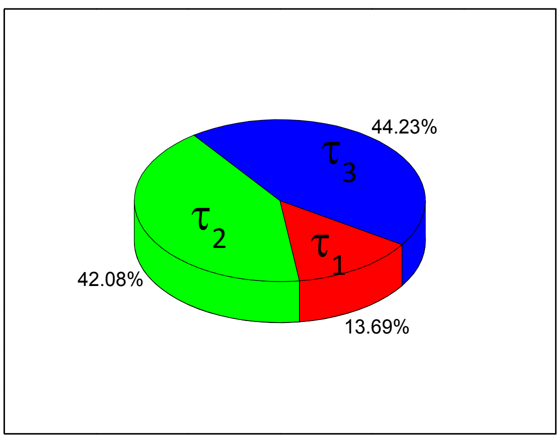

Fractional intensities of the Positive Decay Components

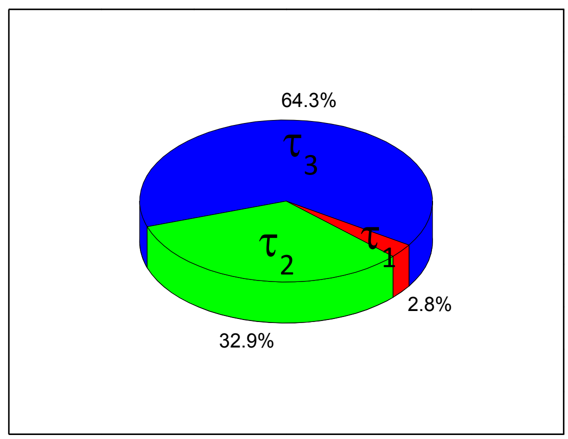

Fractional amplitudes of the Positive Decay Components

Figure 36. Intensity decay of Acridine Orange with the table of fitting parameters. Average intensity and amplitude lifetimes. Pie plots of the fractional intensities and amplitudes for concentration 0.4 mM, 3 pulse exc.

Intensity decay of Acridine Orange with concentration 0.4 mM, excitation 435 nm, emission 640 nm with 3 pulse excitation is presented in Figure 36. Results are similar to the concentration of 1 mM since both intensity average and amplitude average lifetimes decreased in comparison with single pulse excitation. This is caused by increase of fraction of the short component in the decay.

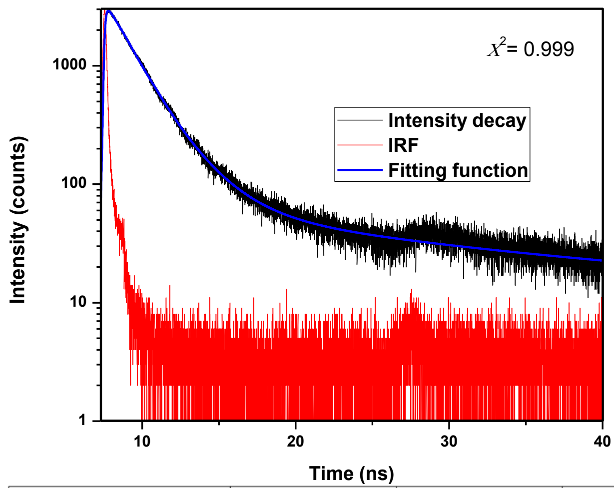

0.2 mM, 1 pulse

Intensity average lifetime:

τ_A =1.914 ns

Intensity average lifetime:

τ_I =2.730 ns

Parameter	Value	Conf. Lower	Conf. Upper	Conf. Estimation
A_1 [Cnts]	221.4	-14.0	+14.0	Fitting
τ_1 [ns]	8.327	-0.376	+0.376	Fitting
A_2 [Cnts]	3732	-103	+103	Fitting
τ_2 [ns]	1.4629	-0.0364	+0.0364	Fitting
A_3 [Cnts]	2383.2	-77.1	+77.1	Fitting
τ_3 [ns]	2.0251	-0.0514	+0.0514	Fitting
Bkgr. Dec [Cnts]	16.083	-0.908	+0.908	Fitting
Bkgr. IRF [Cnts]	2.921	-0.105	+0.105	Fitting
Shift IRF [ns]	-0.00848	-0.00678	+0.00678	Fitting

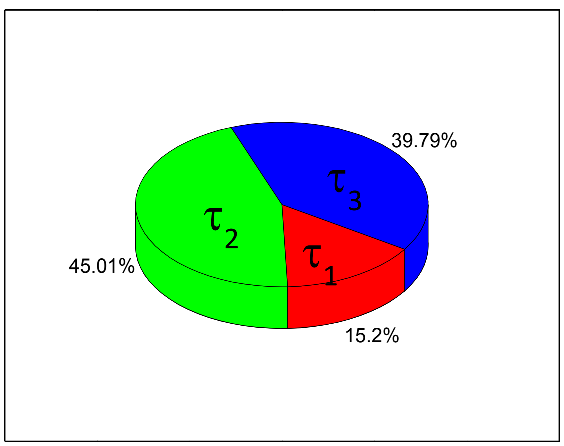

Fractional intensities of the Positive Decay Components

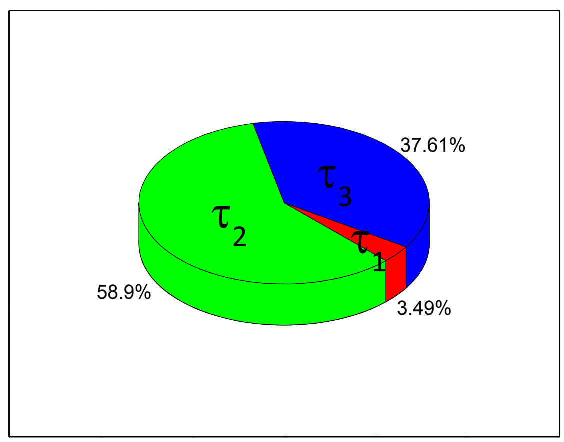

Fractional amplitudes of the Positive Decay Components

Figure 37. Intensity decay of the Acridine Orange with the table of fitting parameters. Average intensity and amplitude lifetimes. Pie plots of the fractional intensities and amplitudes for concentration 0.2 mM, 1 pulse exc.

Figure 37 shows the intensity decay of Acridine Orange with a concentration of 0.2 mM, excited with one pulse at the same excitation and emission wavelength as before. This low concentration, almost a hundred times less than the saturated solution (105 mM) and five times smaller than the previous concentration (0.4 mM), but intensity and amplitude averaged lifetimes are very close to those of the 1 mM with 3 pulse excitation. Multipulse excitation causes decrease of the average lifetime at low concentrations as displayed before.

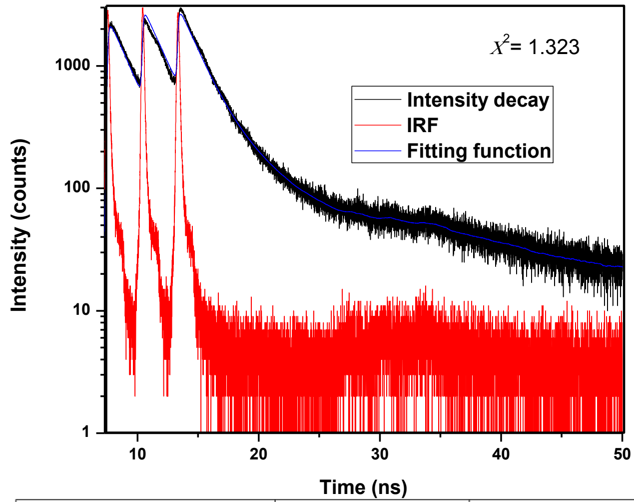

0.2 mM, 3 pulse

Amplitude average lifetime:

τ_A =1.916 ns

Intensity average lifetime:

τ_I =2.843 ns

Parameter	Value	Conf. $_{Lower}$	Conf. $_{Upper}$	Conf. $_{Estimation}$
A_1 [Cnts]	261.1	-23.3	+23.3	Fitting
τ_1 [ns]	9.528	-0.566	+0.566	Fitting
A_2 [Cnts]	2613	-114	+114	Fitting
τ_2 [ns]	2.6897	-0.0931	+0.0931	Fitting
A_3 [Cnts]	7697	-212	+212	Fitting
τ_3 [ns]	1.3951	-0.0368	+0.0368	Fitting
Bkgr. $_{Dec}$ [Cnts]	19.74	-1.48	+1.48	Fitting
Bkgr. $_{IRF}$ [Cnts]	3.749	-0.220	+0.220	Fitting
Shift $_{IRF}$ [ns]	-0.03384	-0.00946	+0.00946	Fitting

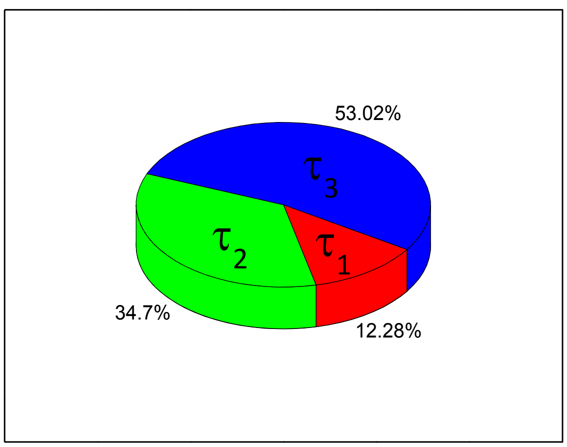

Fractional intensities of the Positive Decay Components

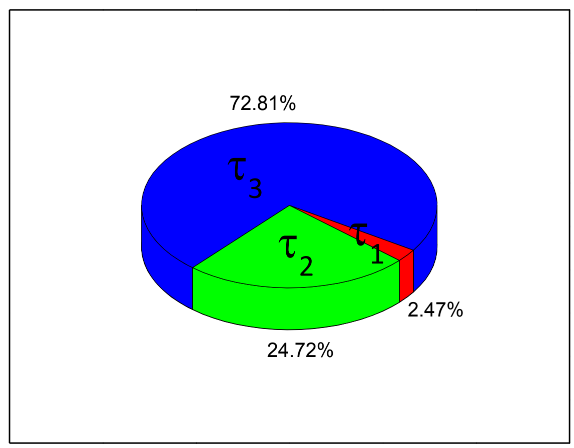

Fractional amplitudes of the Positive Decay Components

Figure 38. Intensity decay of Acridine Orange with the table of fitting parameters. Average intensity and amplitude lifetimes. Pie plots of the fractional intensities and amplitudes for concentration 0.2 mM, 3 pulse exc.

Figure 38 shows a slight increase in the average lifetime of Acridine Orange at a concentration of 0.2 mM excited with 3 pulses. At this concentration there is a slight increase in both intensity and amplitude average lifetimes. This effect is first seen during this set of experiments, since all previously measured concentrations showed a decrease of the average lifetimes. This can be caused by the absence of the interaction at this concentration between aggregates and monomers, since the concentration is low.

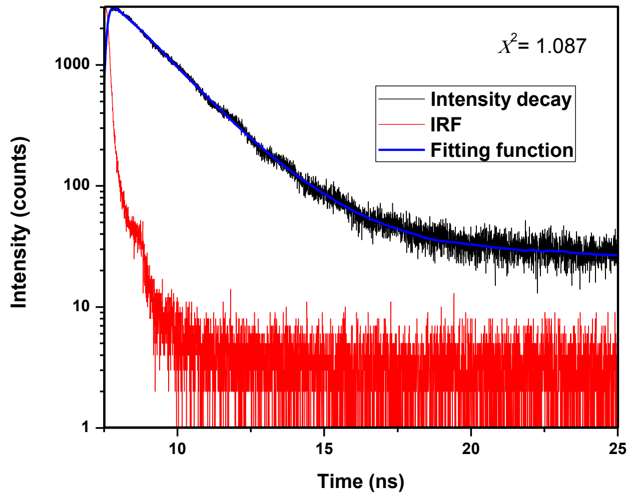

0.1 mM, 1 pulse

Amplitude average lifetime:

τ_A =1.68 ns

Intensity average lifetime:

τ_I =1.86 ns

Parameter	Value	Conf. $_{Lower}$	Conf. $_{Upper}$	Conf. $_{Estimation}$
A_1 [Cnts]	42.0	-11.3	+11.3	Fitting
τ_1 [ns]	8.06	-1.63	+1.63	Fitting
A_2 [Cnts]	4378.7	-89.5	+89.5	Fitting
τ_2 [ns]	1.5086	-0.0257	+0.0257	Fitting
A_3 [Cnts]	2069.2	-71.5	+71.5	Fitting
τ_3 [ns]	1.9162	-0.0491	+0.0491	Fitting
Bkgr. $_{Dec}$ [Cnts]	23.67	-1.04	+1.04	Fitting
Bkgr. $_{IRF}$ [Cnts]	3.030	-0.135	+0.135	Fitting
Shift $_{IRF}$ [ns]	0.01328	-0.00620	+0.00620	Fitting

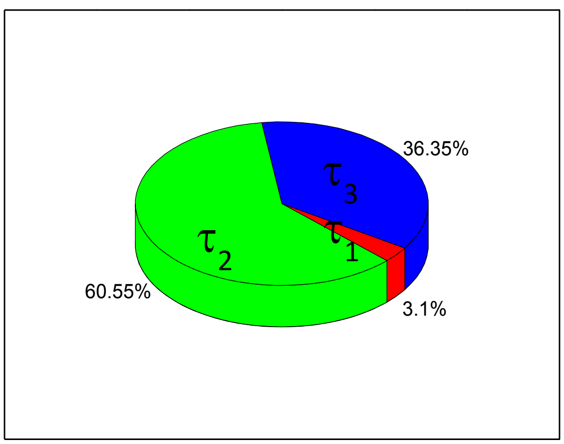

Fractional intensities of the Positive Decay Components

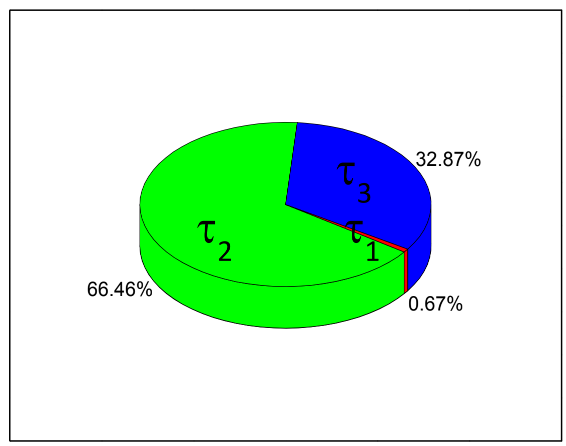

Fractional amplitudes of the Positive Decay Components

Figure 39. Intensity decay of Acridine Orange with the table of fitting parameters. Average intensity and amplitude lifetimes. Pie plots of the fractional intensities and amplitudes for concentration 0.1 mM, 1 pulse exc.

Figure 39 represents the intensity decay of Acridine Orange with a concentration of 0.1 mM. This concentration is low enough that intensity average and amplitude average lifetimes are below the 2 ns lifetimes of the dominant monomer fraction in the solution.

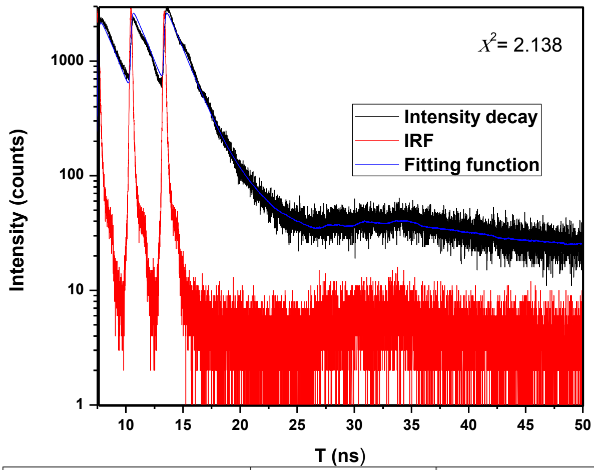

0.1 mM, 3 pulse

Amplitude average lifetime:

τ_A =2.730 ns

Intensity average lifetime:

τ_I =1.914 ns

Parameter	Value	Conf. $_{Lower}$	Conf. $_{Upper}$	Conf. $_{Estimation}$
A_1 [Cnts]	12.57	-8.72	+8.72	Fitting
τ_1 [ns]	21.7	-11.6	+11.6	Fitting
A_2 [Cnts]	9917	-207	+207	Fitting
τ_2 [ns]	1.5128	-0.0282	+0.0282	Fitting
A_3 [Cnts]	978.5	-98.2	+98.2	Fitting
τ_3 [ns]	3.055	-0.208	+0.208	Fitting
Bkgr. $_{Dec}$ [Cnts]	26.83	-1.84	+1.84	Fitting
Bkgr. $_{IRF}$ [Cnts]	4.236	-0.304	+0.304	Fitting
Shift $_{IRF}$ [ns]	0.000	---	---	<none>

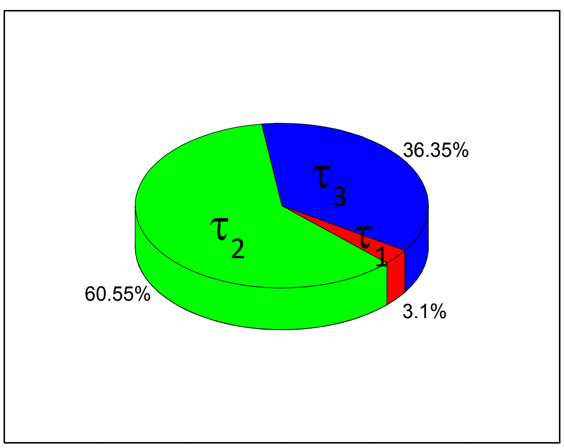

Fractional intensities of the Positive Decay Components

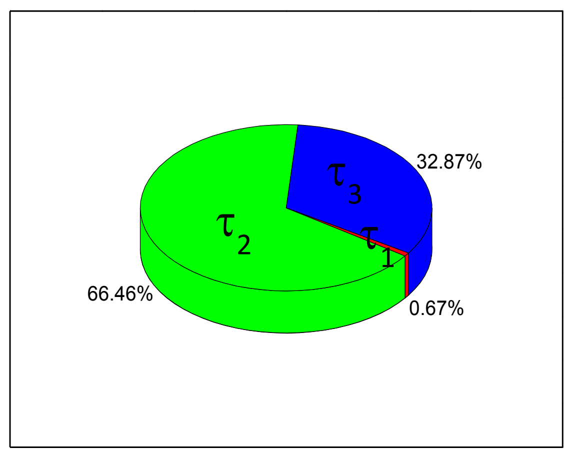

Fractional amplitudes of the Positive Decay Components

Figure 40. Intensity decay of the Acridine Orange with the table of fitting parameters. Average intensity and amplitude lifetimes. Pie plots of the fractional intensities and amplitudes for concentration 0.1 mM, 3 pulse exc.

Figure 40 shows the intensity decay of Acridine Orange at a concentration of 0.1 mM excited with 3 pulses. In comparison with single pulse excitation intensity average lifetime is longer. It can be assumed that interaction of aggregates is low enough at this concentration, they do not quench with each other when they are in the excited state, so there is a slight increase in the intensity average lifetime.

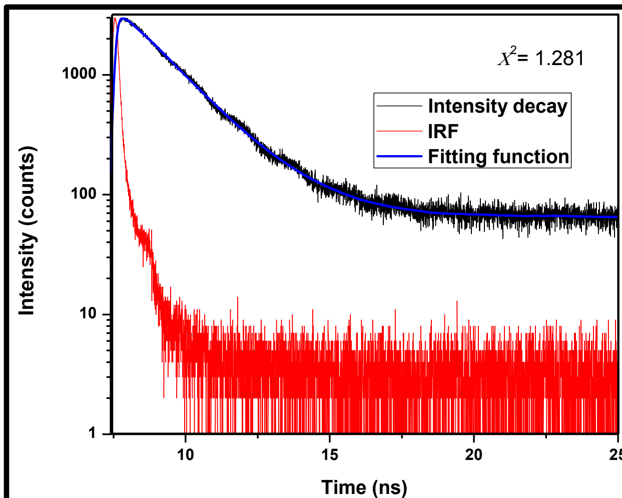

0.02 mM, 1 pulse

Intensity average lifetime:

τ_A =1.86 ns

Amplitude average lifetime:

τ_I =1.68 ns

Parameter	Value	Conf. $_{Lower}$	Conf. $_{Upper}$	Conf. $_{Estimation}$
A_1 [Cnts]	13.4	-26.3	+26.3	Fitting
τ_1 [ns]	3.82	-5.19	+5.19	Fitting
A_2 [Cnts]	3471.0	-65.7	+65.7	Fitting
τ_2 [ns]	1.6359	-0.0257	+0.0257	Fitting
A_3 [Cnts]	2949.1	-65.7	+65.7	Fitting
τ_3 [ns]	1.6350	-0.0302	+0.0302	Fitting
Bkgr. $_{Dec}$ [Cnts]	66.96	-1.87	+1.87	Fitting
Bkgr. $_{IRF}$ [Cnts]	3.311	-0.255	+0.255	Fitting
Shift $_{IRF}$ [ns]	0.01478	-0.00505	+0.00505	Fitting

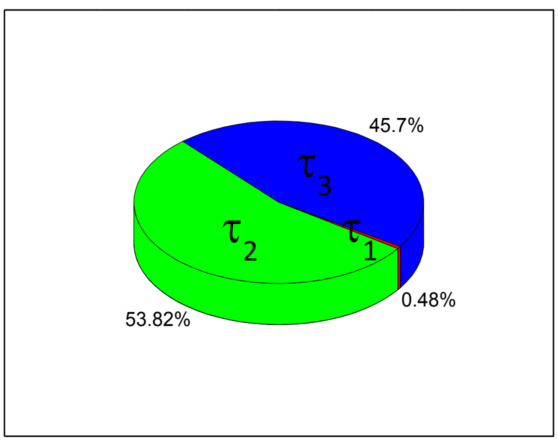

Fractional intensities of the Positive Decay Components

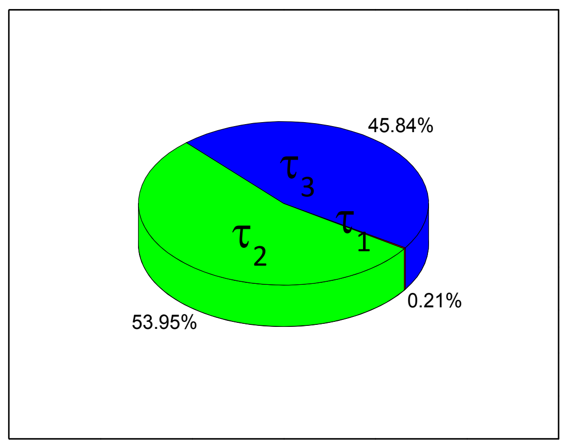

Fractional amplitudes of the Positive Decay Components

Figure 41. Intensity decay of Acridine Orange with the table of fitting parameters. Average intensity and amplitude lifetimes. Pie plots of the fractional intensities and amplitudes for concentration 0.02 mM, 1 pulse exc.

Figure 41 shows the intensity decay of Acridine Orange at a concentration of 0.02 mM excited with a single pulse. The intensity decay can be fitted with a single component, but it was fitted with 3 to see if a small fraction of aggregates are present. In this case fitting with 3 components can be treated as artificial, but intensity and amplitude average lifetimes are short and will be the same as in the case of single component fitting. Intensity and amplitude average lifetimes are extremely close to those of 0.1 mM concentration. It can be concluded that monomers are dominating at this low concentration, regardless of the excitation of 435 nm that excites preferentially aggregates.

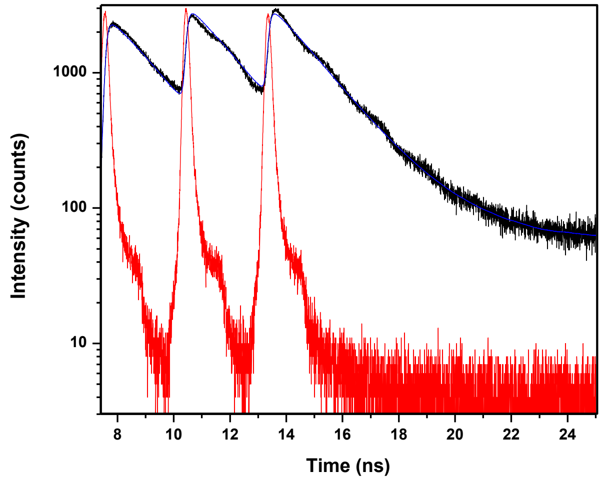

0.02 mM, 3 pulse

Amplitude average lifetime:

τ_A =1.64 ns

Intensity average lifetime:

τ_I =1.66 ns

Parameter	Value	Conf. Lower	Conf. Upper	Conf. Estimation
A_1 [Cnts]	16.2	-36.1	+36.1	Fitting
τ_1 [ns]	4.90	-6.73	+6.73	Fitting
A_2 [Cnts]	7273	-123	+123	Fitting
τ_2 [ns]	1.7315	-0.0253	+0.0253	Fitting
A_3 [Cnts]	3834	-145	+145	Fitting
τ_3 [ns]	1.4552	-0.0501	+0.0501	Fitting
Bkgr. Dec [Cnts]	59.25	-2.02	+2.02	Fitting
Bkgr. IRF [Cnts]	4.020	-0.332	+0.332	Fitting
Shift IRF [ns]	0.01733	-0.00692	+0.00692	Fitting

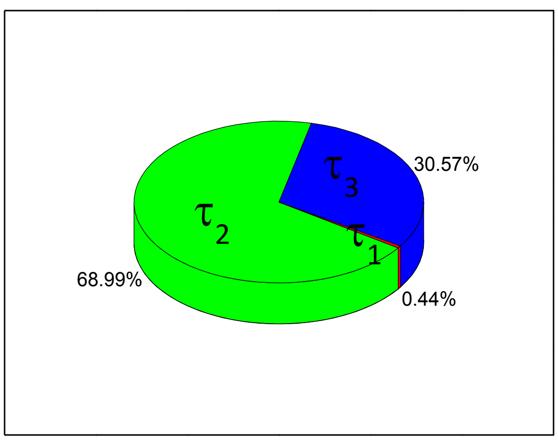

Fractional intensities of the Positive Decay Components

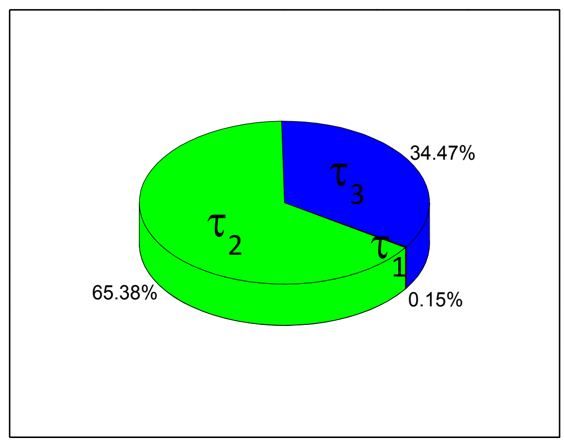

Fractional amplitudes of the Positive Decay Components

Figure 42. Intensity decay of Acridine Orange with the table of fitting parameters. Average intensity and amplitude lifetimes. Pie plots of the fractional intensities and amplitudes for concentration 0.02 mM, 3 pulse exc.

Figure 42 presents intensity decay of Acridine Orange at a concentration of 0.02 mM excited with a single pulse. Decay is also fitted with 3 components, but easily can be fitted with a single one. Intensity average and amplitude average lifetimes are exactly the same as those with single pulse excitation. Monomers dominate at this concentration, so there is no pumping of the aggregates, concentration of 0.1 mM shows this already and 0.02 mM completely certifies this statement.

Emission spectra measurements

We also performed emission spectra measurements in order to see changes between spectra obtained with single pulse excitation and multiple pulses. Figure 43 displays plots of normalized Acridine Orange emission spectra excited with a single pulse and 3 pulses. Concentration are 1 mM, 0.4 mM, 0.2 mM, 0.1 mM and 0.02 mM, excitation wavelength 435 nm.

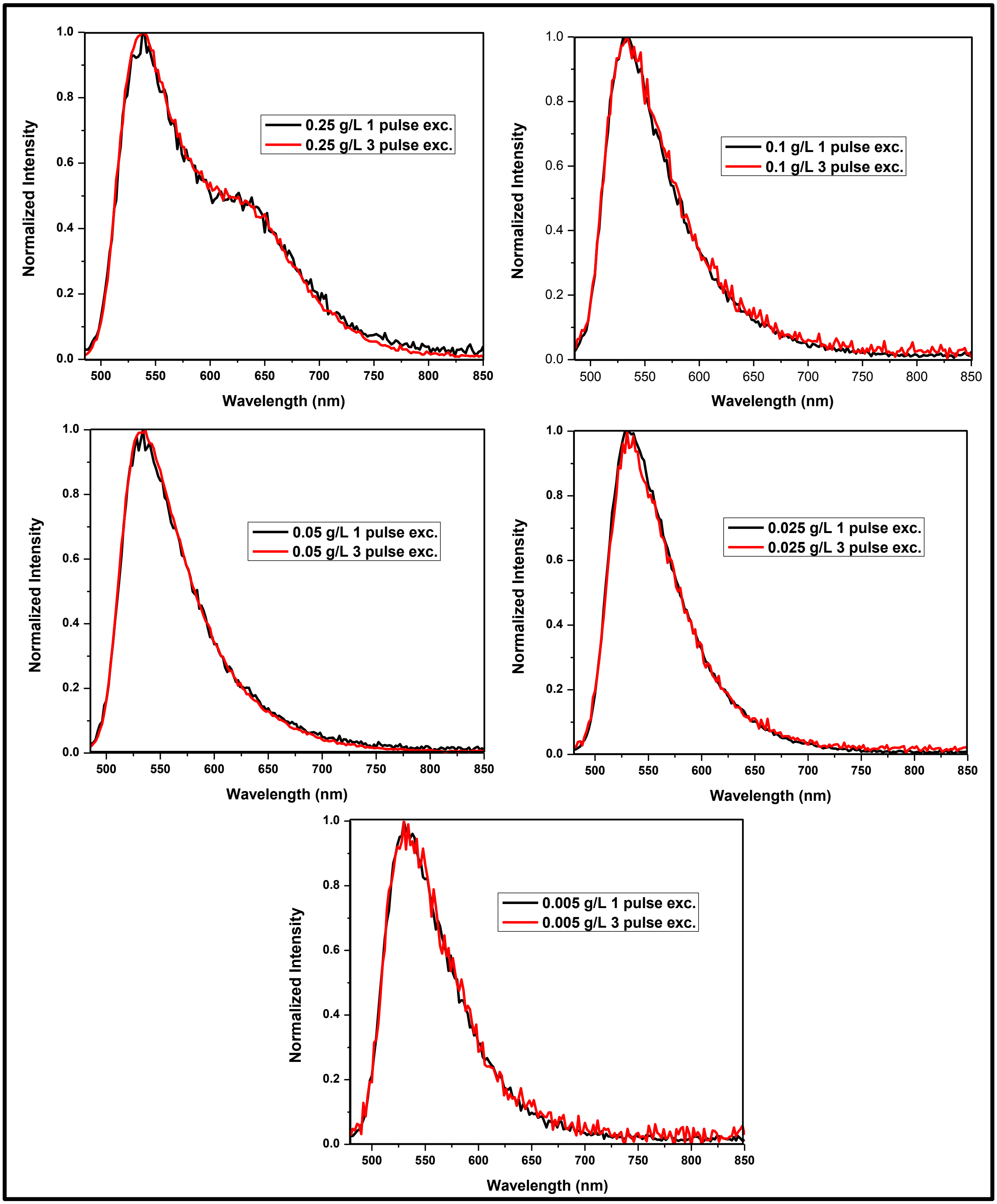

Figure 43. Emission spectra of Acridine Orange collected with 1 and 3 pulse excitation. Excitation wavelength 435 nm.

Emission spectra have similar shape in both cases of excitation for these concentrations. Spectra collected with the single pulse excitation include more background noise, since excitation with the single pulse has lower intensity than the excitation with the 3 pulses. There is no apparent change in the emission spectra, since there is now strong pumping of the aggregates.

Tail fitting results

There is no apparent increase in lifetime of Acridine Orange with the fitting procedure that includes deconvolution of the decay together with fitting to a three exponential model. Because of this we decided to apply global tailfitting. This technique is conventionally used in fluorescence intensity decay measurements. Results of the tailfitting are presented in the table below:

	1 pulse		3 pulse	
Conc. (mM)	FA (11.8 ns)	FA (1.79 ns)	FA (11.8 ns)	FA (1.79 ns)
1	25%	75%	38%	62%
0.4	4%	96%	7%	93%
0.2	3%	97%	6%	94%
0.1	1%	99%	2%	98%

50 ps delay

Table 2. Fractional Amplitudes (FA) of different species presented in Acridine Orange decay (short and long lifetimes). Excitation performed with 1 and 3 pulses.

Excitation with 3 pulses gives an apparent increase in fractional amplitude of the aggregates which have longer lifetimes. A concentration 1mM shows an increase of 13% that is not very large, but lower concentrations show a doubling of the FA of aggregates. This can be caused by dissociation of excited aggregates when they interact during excitation-deactivation process at relatively high concentrations. Lower concentrations have a much higher increase in the amplitude since interaction between excited aggregates is much lower.

Tailfitting is different from conventional fitting, so IRF function and deconvolution is not required for the procedure [43, 56]. We did perform fitting starting with 50 ps delay from the maximum of the function. Delay is needed to avoid negative components in the fit.

	1 pulse		3 pulse	
Conc. (mM)	FI (11.8 ns)	FI (1.79 ns)	FI (11.8 ns)	FI (1.79 ns)
1	68%	32%	79%	21%
0.4	19%	81%	30%	70%
0.2	18%	82%	29%	71%
0.1	4%	96%	9%	91%

50 ps delay

Table 3. Fractional Intensities (FI) of different species presented in the Acridine Orange decay (short and long lifetimes). Excitation performed with 1 and 3 pulses.

Table 3 represents fractional intensities that correspond to multiple concentrations of Acridine Orange excited with 1 and 3 pulses. It also demonstrates an increase in fractional intensities when the sample is excited with 3 pulses. However, increase in fractional intensities is a little bit less than the increase in fractional amplitudes that can be caused by interaction between aggregates during the deexcitation process that lasts up to 15 ns total. On the other hand, a very low concentration of 0.1 mM shows similar behavior to the case of fractional amplitudes. Increase in signal is 5% that more than doubles the total signal up to 9% in comparison single pulse excitation.

Increase in fractional amplitudes is slightly higher than in fractional intensities, that is caused by interactions described above. On the other hand at very low concentrations, the increase in fractional intensities is the same as in the fractional amplitudes (2 times more), but total intensity fraction is dramatically bigger than the amplitude fraction (4% vs 1%, 1 pulse and 9% vs 2% 3 pulse).

As a result of analysis of the intensity decay, both fractional intensities and fractional amplitudes can be obtained. Both of them can be used to determine Acridine Orange concentration from the intensity decay and reveal the increase in sensitivity with the application of multiple pulse excitation. However, fractional intensity analysis can provide more reliable information about the system because they are bigger than the fractional amplitudes and will provide much bigger numerical change between concentrations.

EXPERIMENTL RSULTS, DISCUSSION

Experimental results can provide us with information about the change of the fraction of monomers and aggregates in the solution with the change of concentration. In the introduction it was discussed how Acridine Orange can be used as a dye to study exocytotic processes in the Calu 3 cells. It can accumulate in the cellular vesicles that are transported to the cellular membrane and release into extracellular space together with mucin that unfold and form a uniform layer on the epithelial tissue of the lung. Mucus plays a defensive role in the living organism from the barrage of external viruses and batteries. Figures 13 represent how excitation wavelength was selected from the absorption spectra. It was determined that each specie, has its own preferential excitation wavelength. Aggregates can be excited with 435nm and monomers with 494 nm.

Emission spectra on Figure 14 and 15 showed that aggregates and monomers emit at different wavelength also. Monomers have emission peak around 530 nm and aggregates around 640 nm. From the multiple measurements of different concentration (from 105 g/L to 0.02 mM) it is possible to see that the fraction of aggregates in the solution decreases with the decrease of the concentration. This can allow to monitor differences in mucus exocytotic process of healthy Calu 3 cells and CF – like cells.

Mucus release is a fast process (order of milliseconds) it can be monitored with the microscope in vivo. Measurements of the intensity decays of different concentrations performed during mucosal granula release can help to determine concentration of the mucins at a particular moment.

The extinction coefficient and quantum yield measurements revealed that aggregates have higher extinction coefficient than monomers (around 2-3 times), but they have 10 times lower quantum yield. Moreover, the highest soluble concentration cannot accumulate in the cellular vesicles, only concentrations around 15 mM can accumulate and mucin swelling causes increase in volume few hundred times, low concentration of the Acridine Orange almost do not contain aggregates. We did develop an approach to use multiple pulse excitation to increase the range and resolution of the measurements. We expect that this will help in the productivity of the measurements.

Application of multiple pulse excitation with calculated parameters for the resolution of the aggregates and monomers intensity decays appeared to be useful and can improve the sensitivity of the measurements.

Intensity decays of multiple concentrations that were fitted with 3 exponential decays did not demonstrate any significant change in fluorescent lifetimes as well as fractional intensities and amplitudes. This result was expected and is caused by the fact that the lifetime of the fluorophore is obtained after deconvolution of the lamp function and collected decay. Since the region where all 3 pulses are present is included in the selected fitting region, there shouldn't be any change in the conventionally defined lifetime. Lifetime of the fluorophore will not change, regardless of whether it is excited with the single or 3 pulses in particular case.

Tail fitting doesn't use deconvolution of the collected decay and the lamp function. Fitting can be applied to the slope of the intensity decay starting at any point. Good fitting requires start of the fitting to be close enough to the maximal value of the intensity decay. We tried to follow this statement and applied a delay of only 50 ps to avoid any unexpected negative components of the fit.

Results obtained with tail fitting are dramatically different from those obtained with fitting after deconvolution. Tail fitting is used only at the region where the decaying part of the intensity decay is present. This type of fitting can demonstrate increase of the fraction of the aggregates that have longer lifetime. Fractional intensities and fractional amplitudes of the aggregates grow as a results of this. Fitting results that are presented in the Table 2 and Table 3 demonstrate that excitation with 3 sequential pulses significantly increased the fraction of the long lifetime component in the decay. Fractional amplitudes increase about 2 times as well as fractional intensities, as shown in Table 1 and Table 2. Fractional intensities are a few times bigger than the fractional amplitudes, a result caused by the relatively long lifetime of the aggregates.

It can be concluded that multiple pulse excitation of Acridine Orange can significantly increase the sensitivity of measurements in comparison with classic single pulse excitation. Application of tail fitting together with global fitting reveals possibility to perform analysis of the intensity decays and monitor change of the concentration of Acridine Orange as a function of the fractional intensities and amplitudes.

Application of multiple pulse excitation together with total internal reflection (TIRF) to the fluorescent microscope reveals possibility to monitor concentration change of Acridine Orange in healthy and CF – like or COPD - like cells in vivo. Multiple pulse excitation will significantly increase sensitivity of the measurements and reveal the possibility for a slight extension of the range of measurements. Ratiometric detection discussed in my Master's thesis can be combined with techniques described above. Together with multiple pulse excitation and TIRF it will provide with sufficient information about mucosal granule release process that happens in the range of milliseconds.

REFERENCES:

1. Richards-Kortum R, Sevick-Muraca E. *Quantitative optical spectroscopy for tissue diagnosis*. Annu Rev Phys Chem. 1996;47:555–606.
2. Wagnieres GA, Star WM, Wilson BC. *In vivo fluorescence spectroscopy and imaging for oncological applications*. Photochem Photobiol. 1998;68:603–632.
3. Alexa L. Mattheyses, Sanford M .Simon and Joshua Z. Rappoport. *Imaging with total internal reflection fluorescence microscopy for the cell biologist*. Journal of Cell Science 123, 3621-3628.2010
4. Kobayashi H, Ogawa M, Alford R, Choyke PL, Urano Y. *New strategies for fluorescent probe design in medical diagnostic imaging*. Chem Rev. 2010;110:2620–2640.
5. Andersson-Engels S, Klinteberg C, Svanberg K, Svanberg S. *In vivo fluorescence imaging for tissue diagnostics*. Phys Med Biol. 1997;42:815–824.
6. Rafal Luchowski, Zygmunt Gryczynski, Pabak Sarkar, Julian Borejdo, Mariusz Szabelski, Peter Kapusta, and Ignacy Gryczynski. *Instrument response standard in time-resolved fluorescence*, American Institute of Physics. (DOI: 10.1063/1.3095677).
7. S. E. Webber. *The Role of Time-Dependent Measurements in Elucidating Static Versus Dynamic Quenching Processes*, Photochemistry and Photobiology, 1997, 65(1): 33-38.
8. Marika Savarese, Anna Aliberti, Ilaria De Santo, Edmondo Battista, Filippo Causa, Paolo Antonio Netti, and Nadia Rega. *Fluorescence Lifetimes and Quantum Yields of RhodamineDerivatives: New Insights from Theory and Experiment*, J. Phys. Chem. A, DOI: 10.1021/jp3021485
9. Parker, C. A. and W. T. Rees. *Correction of fluorescence spectra and the measurement of fluorescence quantum efficiency*. Analysr 85. 587-600, (1960)
10. Richards-Kortum R, Sevick-Muraca E. *Quantitative optical spectroscopy for tissue diagnosis*. Annu Rev Phys Chem. 1996;47:555–606.
11. Wagnieres GA, Star WM, Wilson BC. *In vivo fluorescence spectroscopy and imaging for oncological applications*. Photochem Photobiol. 1998;68:603–632.

12. Chorvat D, Chorvatova A. *Multi-wavelength fluorescence lifetime spectroscopy: a new approach to the study of endogenous fluorescence in living cells and tissues*. Lasers Phys Lett. 2009;6:175–193.
13. Kobayashi H, Ogawa M, Alford R, Choyke PL, Urano Y. *New strategies for fluorescent probe design in medical diagnostic imaging*. Chem Rev. 2010;110:2620–2640.
14. Andersson-Engels S, Klinteberg C, Svanberg K, Svanberg S. *In vivo fluorescence imaging for tissue diagnostics*. Phys Med Biol. 1997;42:815–824.
15. Cubeddu R, Comelli D, D'Andrea C, Taroni P, Valentini G. *Time-resolved fluorescence imaging in biology and medicine*. J Phys D: Appl Phys. 2002;35:R61–76.
16. Zipfel WR, Williams RM, Christie R, Nikitin AY, Hyman BT, Webb WW. *Live tissue intrinsic emission microscopy using multiphoton-excited native fluorescence and second harmonic generation*. Proc Natl Acad Sci U S A. 2003;100:7075–7080.
17. Thekkek N, Richards-Kortum R. *Optical imaging for cervical cancer detection: solutions for a continuing global problem*. Nat Rev Cancer. 2008;8:725–731.
18. McGinty J, Galletly NP, Dunsby C, Munro I, Elson DS, Requejo-Isidro J, Cohen P, Ahmad R, Forsyth A, Thillainayagam AV, Neil MAA, French PMW, Stamp GW. *Wide-field fluorescence lifetime imaging of cancer*. Biomed Opt Expres. 2010;1:627–640.
19. Redden Weber C, Schwarz RA, Atkinson EN, Cox DD, Macaulay C, Follen M, Richards-Kortum R. *Model-based analysis of reflectance and fluorescence spectra for in vivo detection of cervical dysplasia and cancer*. J Biomed Opt. 2008;13:064016.
20. Bajzer Z, Prendergast FG. *A model for multiexponential tryptophan fluorescence intensity decay in proteins*, Biophys J. 1993 Dec;65(6):2313-23.
21. Eftink, M. R. *The use of fluorescence methods to mon itor unfolding transitions in proteins*. Biophys. J. 66, 482-50 (1994)
22. Hennecke, J., A. Sillen, M. Huber-wunderlich. Y. Engelborghs and R. Glockshuber. *Quenching of tryptophan fluorescence by the active-site disulfide bridge in the DsbA protein from Escherichia coli*. Biochemistry 36, 639 1-6400., doi:10.1039/F19736900056. (1997)
23. Prendergast F, Mann K (1978). *Chemical and physical properties of aequorin and the green fluorescent protein isolated from Aequorea victoria*. Biochemistry 17 (17): 3448–53. doi:10.1021/bi00610a004. PMID 28749

24. Gonçalves S1, Santos NC, Martins-Silva J, Saldanha C. *Fibrinogen-beta-estradiol binding studied by fluorescence spectroscopy: denaturation and pH effects*. J Fluoresc. 2006 Mar;16(2):207-13.
25. Rama Bansil, Bradley S. Turner. *Mucin structure, aggregation, physiological functions and biomedical applications*, Expert Opin Investig Drugs. 2002 Jan;11(1):15-35.
26. Kagnoff , M . F . & Eckmann .*Epithelial cells as sensors for microbial Infection*, J. Clin. Invest. 100 , 6 – 10 (1997) .
27. Lu , J . , Teh , C . , Kishore , U . & Reid , K . B . *Collectins and fi colins: sugar pattern recognition molecules of the mammalian innate immune system*, Biochim. Biophys. Acta 1572 , 387 – 400 (2002) .
28. Raj , P . A . & Dentino , A . R . *Current status of defensins and their role in innate and adaptive immunity* . FEMS Microbiol. Lett. 206 , 9 – 18 (2002) .
29. Mercer RR ML , R . & Crapo , J . D . *Mucous lining layers in human and rat airways* . Ann. Rev. Resp. Dis. 145 , 355 (1992)
30. Jordan , N . , Newton , J . , Pearson , J . & Allen , A . *A novel method for the visualization of the in situ mucus layer in rat and man* . Clin. Sci. (London) 95 , 97 – 106 (1998) .
31. Rogers DF. *Mucus hypersecretion in chronic obstructive pulmonary disease*, Novartis Found Symp. 2001;234:65-77; discussion 77-83.
32. Sawicki, G.S. | Sellers, D.E. | Robinson, W.M. *High treatment burden in adults with cystic fibrosis: Challenges to disease self-management,* Journal of Cystic Fibrosis, Elsvsir,Volume 8, Issue 2, March 2009, Pages 91-96.
33. DAVID TINKELMAN, MD; ROBERT J. NORDYKE, PhD; SHARON ISONAKA, MD; DOROTHY GEORGE, PharmD; KEITH DESFOSSES, MBA; and DMITRY NONIKOV, MD. *The Impact of Chronic Obstructive Pulmonary Disease on Long-term Disability Costs*, Manag Care Pharm. 2005:11(1):25-32
34. Shumilov D, Popov A, Fudala R, Akopova I, Gryczynski I, Borejdo J, Gryczynski Z, Grygorczyk R. *Real-time imaging of exocytotic mucin release and swelling in Calu-3 cells using acridine orange*, Methods. 2013 Sep 18. pii: S1046-2023(13)00364-2. doi: 10.1016/j.ymeth.2013.09.004
35. Rogers DF. *Mucoactive agents for airway mucus hypersecretory diseases*, Respir Care. 2007 Sep;52(9):1176-93; discussion 1193-7.
36. Brian Button, Li-Heng Cai, Camille Ehre, Mehmet Kesimer, David B. Hill, John K. Sheehan, Richard C.Boucher, Michael Rubinstein. *A Periciliary Brush Promotes the Lung Health by Separating the Mucus Layer from Airway Epithelia*. Science Vol.337, 24 August 2012
37. Alfred M.Lucas, Ph.D.; L.Douglas, *Principles underlying ciliary activity in the respiratory tract.II.A comparison of nasal clearance in man, monkey and*

other mammals, Arch Otolaryngol. 1934;20(4):518-541. doi:10.1001/archotol.1934.03600040074006

38. Houtmeyers E1, Gosselink R, Gayan-Ramirez G, Decramer M. *Regulation of mucociliary clearance in health and disease.* Eur Respir J. 1999 May;13(5):1177-88.

39. Ryan M Rich, Ignacy Gryczynski, Rafal Fudala, Julian Borejdo, Dorota L Stankowska, Raghu R Krishnamoorthy, Sangram Raut, Badri P Maliwal, Dmytro Shumilov, Hung Doan, Zygmunt Gryczynski. *Multiple-pulse pumping for enhanced fluorescence detection and molecular imaging in tissue, DOI:10.1016/j.ymeth.2013.08.026. Source: PubMed*

40. Shohren Nafisi, Ali Akbar Saboury, Nahid Keramat, Jean-Francois Neault, Heidar-Ali Tajmir-Riahi. *Stability and structural features of DNA intercalation with ethidium bromide, acridine orange and methylene blue*. Journal of Molecular Structure, May 2006

41. B. H. Robinson, A. Lofflera, G. Schwartz. *Thermodynamic Behaviour of Acridine Orange in Solution*, doi:10.1039/F19736900056.

42. Rudolf Suttinger and Frank Strohbusch. *Acid Base Reactions Between Acridine Orange and Substituted Phenols in Benzonitrile Part 11. Kinetics: An Extended Eigen Mechanism of Proton Transfer*, Phys. Chem. 88, 750-759 (1984)

43. Joseph R.Lakowich. *Principles of Fluorescence Spectroscopy, Second edition*. ISBN 0-306-46093-9, 1999 Kluwer Academic/ Plenum Publishers, New York, 10-11 pp.

44. O.S.Wolbeis, M.Hof, R.Hutterer, V.Fidler, *Fluorescent Spectroscopy in Biology*, ISBN 3-540-22338-X, 105p.

45. Joseph R.Lakowich. *Principles of Fluorescence Spectroscopy, Second edition.* ISBN 0-306-46093-9, 1999 Kluwer Academic/ Plenum Publishers, New York, 96 p.

46. Mikhail Y. Berezin and Samuel Achilefu. *Fluorescence Lifetime Measurements and Biological Imaginag*. Chem.-Rev.,2010,10,2641-26-84

47. Wolfgang Becker, *TCSPC Handbook, 4th edition*. Becker & Hickl GmbH 2010, p.39

48. Yi Chun-Chen, Robert M Clegg, *Fluorecence lifetime-resolved imaging* Photosynth Res (2009) 102:143-155

49. Philip R. Bevington. *Data Reduction and Error Analysis in Physical Sciences*. McGraw – Hill Book Company 1969

50. Joseph R.Lakowich. *Principles of Fluorescence Spectroscopy, Second edition*. ISBN 0-306-46093-9, 1999 Kluwer Academic/ Plenum Publishers, New York, 119-120 pp.

51. Michael E.Lamn and David M.Neville. *The Dimer Spectrum of Acridine Orange Hydrochloride*. The Journal of Physical Chemistry, Volume 69,Number 11, November 1965
52. P.Verdugo. *Supramolecular Dynamics of Mucus*. Cold Spring Harb Med 2012;2:a009597
53. *COPD*, American Lung Association website
54. *CF*, American Lung Association website
55. *PicoQuant FT 300 brochure* (PicoQuant website)
56. S. Pelet, M. J. R. Previte, L. H. Laiho, and P. T. C. So. *A Fast Global Fitting Algorithm for Fluorescence Lifetime Imaging Microscopy Based on Image Segmentation*, Biophysical Journal Volume 87 October 2004 2807–2817

VITA

PERSONAL

Dmytro Shumilov
Gorlovka, Ukraine
02-February-1989

EDUCATION

August 2010 – present — TCU, Department of Physics and Astronomy, graduate srudent

Sep. 2006-June 2010 — Kharkiv National University

Department of Physics and Technology.
Chair of Physical Technology
Bachelor of Science, Physics

PROFESSIONAL EXPERIENCE

01 July –
01 September 2009 — Practical experience in the Research lab of the Department of Physical Technologies, working with vacuum equipment.

01 September 2009 –
30 June 2010 — Science Center "Kharkov National University". Work on problems concerning supercooling during crystallization of thin island films.

1 April 2010 – 30 June 2010	Science Center “Kharkov National University”, Laboratory of Microstructure Investigation. Laboratory technician.
20 August 2010 – present	Department of Physics and Astronomy, research assistant, teaching assistant

ABSTRACT

APPLICATION OF MULTIPULSE EXCITATION TO STUDY EXOCYTOTIC PROCESSES IN CELLS STAINED WITH ACRIDINE ORANGE

By Dmytro Shumilov, Ph.D., 2014
Department of Physics and Astronomy
Texas Christian University

Thesis Advisor:

Dr. Zygmunt (Karol) Gryczynski, Professor – Physics Biomedical

Mucus secretion is the first-line of defence against the barrage of irritants inhaled into human lungs, but abnormally thick and viscous mucus results in many respiratory diseases. Investigation of processes underlying mucus pathology is hampered, in part, by lack of appropriate experimental tools for labeling and studying mucin granule secretion from live cells with high sensitivity and temporal resolution. Fluorescence spectra and fluorescence lifetime of AO measurements reveal significant changes due to aggregation, and this properties can be useful for determination of mucus expansion.

In particular report I introduce an original technique that enchances quality of the exocytotic process study in Calu 3 cells. Multi - pulse excitation significantly increases number of excited aggregates at low concentration of Acridine Orange that reveals possibility to monitor lower concentration than with classic single

pulse excitation. Increase of the signal strength increases sensitivity of measurements that is very important for the detection of small concentrations (up to nanomolars).